Received: 26 February 2022 | Revised: 28 June 2022 | Accepted: 15 July 2022

DOI: 10.1111/bre.12700

Basin Research | IAS EAGE | WILEY

RESEARCH ARTICLE

Fill-and-Spill, Tilt-and-Repeat (FaSTaR) cycles: Stratigraphic evolution above a dynamic submarine stepped slope

Junia Casagrande[1,2] | **David M. Hodgson**[1] | **Jeff Peakall**[1] | **Pedro Monteiro Benac**[2]

[1]Stratigraphy Group, School of Earth and Environment, University of Leeds, Leeds, UK

[2]Petrobras S. A., Rio de Janeiro, Brazil

Correspondence
Junia Casagrande, Stratigraphy Group, School of Earth and Environment, University of Leeds, Leeds, UK.
Email: eejc@leeds.ac.uk, junia.casagrande@petrobras.com.br

Funding information
Petrobras S.A., Brazil

Abstract

The classic fill-and-spill model is widely applied to interpret topographic controls on depositional architecture and facies distributions in slope successions with complicated topography. However, this model implies a constant topographic configuration over the lifespan of a turbidite system. In contrast, the impact on patterns of erosion and deposition above dynamic slopes whose topographic configuration varies spatially over time remains poorly investigated. Here, using high-resolution 3D seismic reflection data and more than 100 wells from a 40 km long stepped slope system (Campos Basin, offshore Brazil), we document the evolution of a sand-prone turbidite system active during the Oligocene–Miocene transition. This turbidite system was influenced by vertical and lateral deformation, and we propose a new stratigraphic model to explain the resultant depositional architecture. Two depocentres were identified as steps, with channels on the proximal step, and channel–lobe complexes on the distal step, bounded by sediment bypass-dominated ramps. Lateral stepping of channels on the proximal step, and oblique stacking of the down-dip lobe complexes, each cut by through-going channels, indicate multiple fill-and-spill cycles. A persistent north-east-ward stepping and thickening on the steps are interpreted to reflect lateral tilting of the seafloor driven by salt tectonics. The dynamic substrate prevented the establishment of a single long-lived conduit across the proximal step, as recorded in systems with fixed topographic configurations. The filling of through-going channels with mud at the end of each cycle suggests waxing-to-waning sediment supply cycles and periods of sand starvation when the lateral tilting dominated and drove avulsion of the feeder channels towards topographic lows. This study demonstrates that subtle dynamic slope deformation punctuated by discrete sediment supply cycles results in complex stratigraphic patterns with multiple phases, and multiple entry and exit points. Repeated cycles of fill-and-spill, tilt-and-repeat are likely to be present in other stepped slope systems.

KEYWORDS

3D seismic geomorphology, Campos Basin, fill-and-spill model, salt tectonics, stepped slopes, submarine channels and lobes, turbidite systems

1 | INTRODUCTION

Intra-slope depocentres are sites of sediment storage that record important information about the evolution of submarine slope systems, the interaction of sediment gravity flows with slope topography and the stratigraphic connection between shallow- and deep-water environments. In addition, these areas are prone to significant sand accumulation and host economically important hydrocarbon reservoirs (e.g., Booth et al., 2003; Prather, 2003; Prather et al., 2009, 2012). According to the topographic configuration, intra-slope depocentres range from three-dimensional confined basins that record ponded accommodation (sensu Prather, 2003) to stepped profiles that comprise lower gradient steps with healed accommodation (sensu Prather, 2003), connected through higher gradient ramps.

Intra-slope confined basins have been widely documented in salt withdrawal basins that display high rates of salt mobility (e.g., Beaubouef & Friedmann, 2000; Booth et al., 2003; Doughty-Jones et al., 2017; Pirmez et al., 2000; Prather, 2000, 2003; Prather et al., 1998, 2012; Smith, 2004; Winker, 1996) and emplacement of mass transport complexes (e.g., Cumberpatch et al., 2021; Wu et al., 2020). Stepped profiles have been associated with low rates of slope deformation and average sedimentation rates (Hay, 2012; Meckel et al., 2002) and exhibit subtle gradient changes (Brooks et al., 2018; Mignard et al., 2019), where sedimentation rates outpace deformation rates (Adeogba et al., 2005; Deptuck et al., 2012; Hay, 2012; Pirmez et al., 2000; Prather, 2003). Accommodation creation has been attributed to several factors such as salt tectonics (Hay, 2012; Smith, 2004), mud diapirism (Adeogba et al., 2005; Barton, 2012; Deptuck et al., 2012; Jobe et al., 2017), scars of mass transport complexes (Spychala et al., 2015) and differential compaction and subsidence (Brooks et al., 2018; Jackson et al., 2008; Spychala et al., 2015). In salt basins, stepped profiles have been related to complex topographic settings such as connected tortuous corridors formed by discontinuous salt-cored structures (Hay, 2012; Howlett et al., 2021; Oluboyo et al., 2014; Prather, 2003; Smith, 2004). Salt-influenced depocentres usually display pronounced salt-cored structures, such as massive salt walls and diapirs, typical of zones of structural shortening where salt thickens in contractional salt domains (Demercian et al., 1993; Howlett et al., 2021; Mayall et al., 2010). In these settings, submarine channels diverge around, or converge towards, constriction points between salt structures, from where distributary systems emanate into less-confined lower gradient slope sectors. However, the depositional patterns of intra-slope depocentres affected by modest salt-related structural relief remain poorly investigated.

Highlights

- Connected submarine channel and lobe systems were deposited above a stepped slope in Campos Basin, offshore Brazil
- 3D complex slope topography was controlled by extensional salt tectonics and differential compaction
- Stratigraphic patterns revealed a unidirectional migration trend and multiple fill-and-spill cycles
- Lateral slope tilting drove vertical and lateral accommodation during deposition across the stepped profile
- The stratigraphic evolution was controlled by sediment supply fluctuations and a dynamic slope topography

Despite the majority of documented intra-slope depocentres forming in mobile slopes, the understanding of their stratigraphic evolution has relied on the classic fill-and-spill model. This model predicts a cycle of accommodation filling followed by incision and bypass in depocentres that are not deformed, or are mobile about the vertical axis, during the lifespan of a turbidite system (e.g., Beaubouef & Friedmann, 2000; Sinclair & Tomasso, 2002; Smith, 2004; Pirmez et al., 2000; Prather, 2000, 2003; Prather et al., 1998; Winker, 1996). This model has been applied in stepped slope systems such as intra-slope submarine fans (Jobe et al., 2017), transient fans (Adeogba et al., 2005) and slope aprons (Barton, 2012). In addition, the stratigraphic architecture of fill-and-spill cycles with vertical deformation has been modelled by several authors (e.g., Christie et al., 2021; Sylvester et al., 2015; Wang et al., 2017). In cases where fill-and-spill cycles are vertically stacked, the stratigraphic cyclicity is attributed to the interaction of sediment input and vertical accommodation rejuvenation created by dynamic seafloor deformation induced by fixed structural elements (e.g., Booth et al., 2003; Brooks et al., 2018; Hay, 2012; Spychala et al., 2015). However, accommodation patterns can be spatially variable during the lifespan of a turbidite system, for instance due to basinward tilting (Jackson et al., 2021), lateral tilting (Kane et al., 2010, 2012) and the emplacement of mass-transport complexes (Wu et al., 2020). These factors drive spatially variable topographic configurations and hinder vertical stacking across sediment supply cycles, suggesting that alternative stratigraphic models to the traditional fill-and-spill model need to be developed.

This work investigates the stratigraphic evolution of a sand-prone turbidite unit deposited on the Oligocene–Miocene slope of the Campos Basin, offshore Brazil. This turbidite unit evolved above a stepped slope, with low relief, that exhibited complex topography influenced by extensional salt tectonics and differential compaction. Extensive seismic stratigraphic mapping and well data analysis were carried out in order to: (i) characterise the depositional systems and link the spatial variability in architecture, thickness and sand distribution with seafloor topography; (ii) define a high-resolution stratigraphic framework across the stepped profile; (iii) interpret how slope topography influenced the stratigraphic evolution of the study unit and (iv) propose a high-resolution stratigraphic model for turbidite system evolution above dynamic stepped profiles.

2 | REGIONAL GEOLOGICAL SETTING

The study area is located in the central part of Campos Basin, offshore Brazil, more than 120 km from the coastline in water depths ranging from 600 to 2000 m (Figure 1a). The Campos Basin is located on the Eastern Brazilian Continental Margin, covering an area of 115,000 km^2, mostly offshore of Rio de Janeiro (RJ) and Espírito Santo (ES) states (Figure 1a). The Cabo Frio High defines the southern margin, and the Vitoria High defines the northern margin (Mohriak et al., 1998; Winter et al., 2007), with a small onshore portion to the west (Bruhn et al., 2003) (Figure 1a). The Campos Basin, presently a passive margin, originated from the break-up of the Gondwana supercontinent during the Upper Jurassic/Lower Cretaceous (Chang et al., 1992; Fetter et al., 2009) and is infilled with a 9000 m thick sedimentary succession (Guardado et al., 2000). Three main megasequences form the stratigraphy of Campos Basin: non-marine rift megasequence, transitional megasequence and marine megasequence (Guardado et al., 2000) (Figure 1b,c). Winter et al. (2007) named these sequences as rift, post-rift and drift, respectively. The rift megasequence (Upper Neocomian to Lower Aptian) relates to the Mesozoic break-up process, with rift depocentres infilled by volcanic and continental sediments (Guardado et al., 2000; Winter et al., 2007). Coarse siliciclastic sediments and microbial carbonates overlain by evaporites deposited from the Middle to Upper Aptian record the transition from continental to marine environments during a tectonically mild post-rift stage, forming the transitional or post-rift megasequence (Guardado et al., 2000; Winter et al., 2007). The marine or drift megasequence (Albian to present) evolved in a context of thermal subsidence and salt tectonics and presents a transgressive–regressive trend of marine sedimentation (Guardado et al., 2000; Winter et al., 2007). This megasequence records at its base a shallow-water carbonate platform that was progressively drowned due to thermal subsidence and eustatic sea-level rise (Bruhn, 1998), leading to the deposition of widespread siliciclastic and hemipelagic deep-water sedimentation up to the Upper Cretaceous/Palaeocene (Chang et al., 1992; Guardado et al., 2000; Winter et al., 2007) (Figure 1b). The regressive phase (Palaeocene to present) was driven by increased sediment supply and eustatic sea-level fall, characterised by the progradation of synchronous depositional systems composed of shallow-water carbonates, siliciclastic paralic and deep-water systems (Bruhn, 1998; Winter et al., 2007) (Figure 1b). This study focuses on a deep-water sand-prone interval, informally named here the Marlim unit. This unit forms part of the regressive phase of the Marine/Drift megasequence and was deposited during the Oligocene–Miocene transition (ca. 23 Ma), which coincides with a transient global cooling event associated with ice sheet expansion in Antarctica (Beddow et al., 2016) (Figure 1b,c).

The Campos Basin basement is characterised by northeast (NE)–south-west (SW) and north-west (NW)-southeast (SE) trending horst and graben structures bounded by normal antithetic and synthetic faults developed during the rift phase (Castro & Piccolini, 2015; Guardado et al., 2000; Figure 1c). Post-rift thermal subsidence tilted the passive margin, inducing early stage seaward flow of the Aptian salt (Cobbold & Szatmari, 1991; De Gasperi & Catuneanu, 2014; Quirk et al., 2012). As marine sedimentation progressed, gravity spreading of the overburden enhanced salt mobility (Mohriak et al., 2008). Post-Albian time is characterised by widespread salt tectonics (Mohriak et al., 2008), associated with the formation of a detachment surface at the base of the Aptian Salt (Fetter, 2009). However, post-rift reactivation of the basement fabric is documented, and coupling between basement reactivation structures and salt tectonics can be observed in structural highs (Fetter, 2009).

Two salt tectonic domains are recognised down the basin margin: (i) an up-dip extensional salt-thinned domain characterised by salt rollers, rafts, extensional anticlines, salt pillows and associated normal faults and (ii) a down-dip compressional salt-thickened domain where diapirs, salt walls/ridges and compressional salt tongues are documented (e.g., Cobbold & Szatmari, 1991; Demercian et al., 1993; Fetter, 2009; Mohriak et al., 2008). An intermediate domain between the extensional and compressional domains is described as the transitional domain (Mohriak et al., 2012) or multiphase domain (do Amarante et al., 2021) and shows variable deformation styles. The Marlim unit sits in the extensional

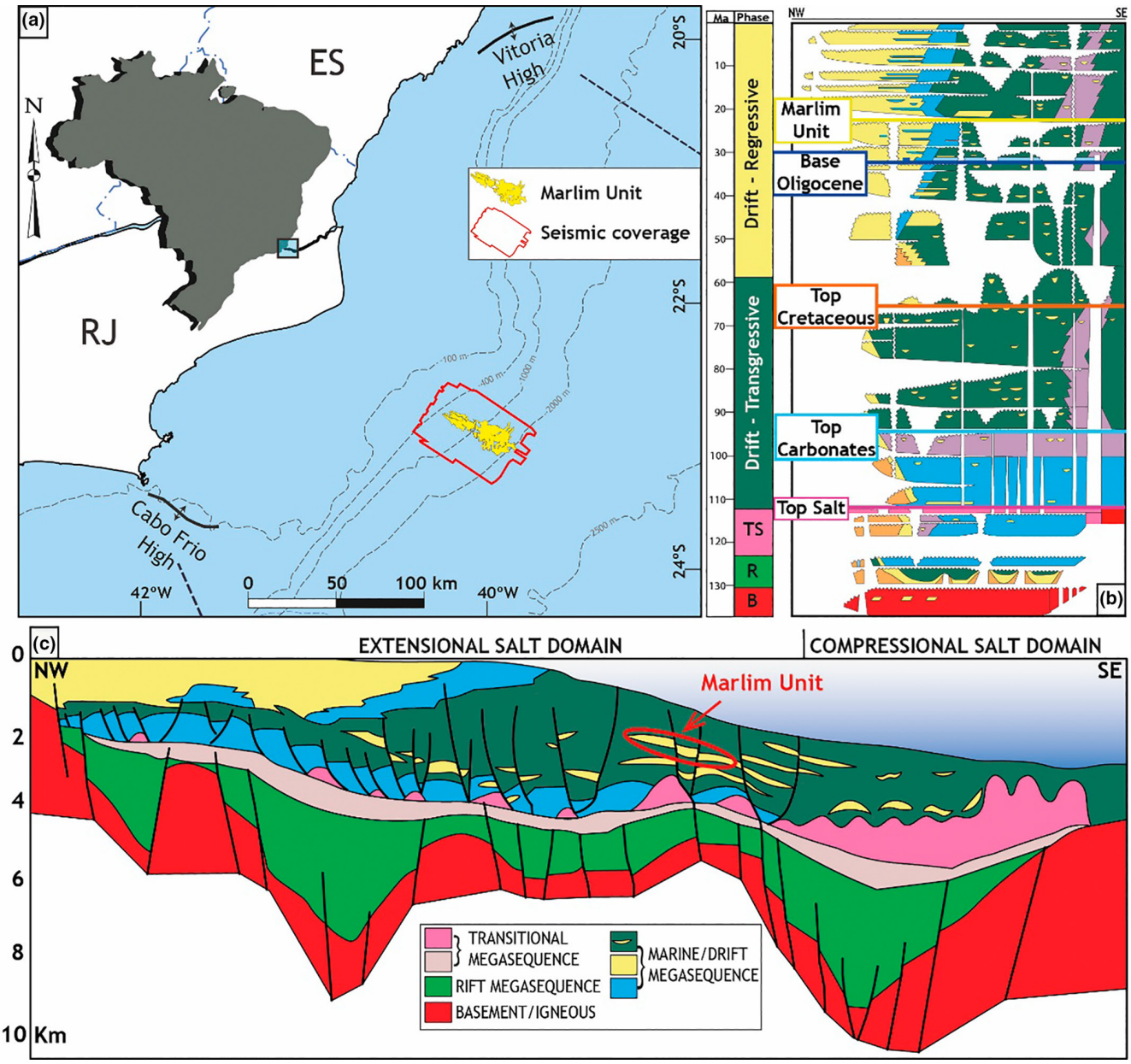

FIGURE 1 (a) Location map of Campos Basin and the Marlim unit study area in the central area of the basin (modified after Bruhn et al., 2017). Inset map of Brazil at the top left with a blue box showing the location of the rest of the figure. ES, Espirito Santo state; RJ, Rio de Janiero state. (b) Stratigraphic chart of Campos Basin with the main stratigraphic phases (megasequences; modified after Winter et al., 2007). The seismic horizons used in this study are named at the left. The top carbonates include the Cenomanian marl interval. Key for lithologies in the stratigraphic chart of (b): red for basement, green for mudstones, yellow for sandstones, orange for conglomerates, blue for carbonates, pink for evaporites and pale purple for marls. In the column phases of the chart, b refers to basement, R to rift and TS to transitional (see text for explanation). (c) Schematic geological dip section representing the stratigraphic framework and the structural style of Campos Basin (modified after Guardado et al., 2000; Rangel & Martins, 1998). The Marlim unit position in the geological section is marked in the red ellipse and sits above the extensional salt domain.

domain, where salt-cored listric normal faults record large amounts of downslope extension related to the stretching and fragmentation of the Albian-Cenomanian carbonate interval (raft tectonics phase, e.g., Demercian et al., 1993; Quirk et al., 2012) (Figure 1c). The bulk of the extension had occurred by the end of the Albian (Quirk et al., 2012). However, salt tectonics continued to be active during the Upper Cretaceous and Cenozoic (Cobbold & Szatmari, 1991; Demercian et al., 1993; Fetter, 2009).

Salt tectonics plays a key role in deep-water sedimentation patterns in the Campos Basin. Salt-related seafloor deformation controlled accommodation patterns on the slope, leading to the accumulation of large volumes of sand-prone turbidites from the Upper Cretaceous

to the Neogene (e.g., Albertão et al., 2011; Cainelli & Mohriak, 1999; Guardado et al., 2000; Winter et al., 2007). These slope turbidite systems, such as the Marlim unit, form prolific hydrocarbon reservoirs. Therefore, there is an abundance of seismic reflection and core/well data. These data permit more in-depth study of mobile substrates and deep-water sediment transport and deposition patterns.

3 | DATA SET AND METHODS

This study uses a comprehensive subsurface data set comprising multiple 3D high-resolution seismic reflection volumes, 110 wells with basic wireline logs and 231.3 m of core from 12 wells. The full-stack seismic volume is a merge of two different volumes, acquired in 1999 and 2010. The merged volume was processed as a pre-stack time migration (PSTM) in 2014 to generate a single volume that covers the whole study area. The bin size spacing is 12.5 m for inlines and crosslines, and the vertical sampling is 4 ms. The average seismic frequency in the Oligocene–Miocene interval is around 30 Hz, resulting in a vertical resolution of approximately 22 m (using an interval velocity of 2650 ms from an average obtained with sonic logs), although thinner events can be detected. A higher resolution 3D PSTM volume processed in 2006 (bin size 12.5 m for inlines and 6.25 m for crosslines and 2 ms for vertical sampling), which covers part of the study area, was used to check interpretations in areas of structural complexity.

Both seismic reflection data sets were processed to zero-phase wavelet and are shown with SEG normal polarity. A negative reflection coefficient is linked to a trough and indicates a decrease in acoustic impedance (check Marlim unit top, Figure 2). The Marlim unit contains oil-saturated high porosity sandstones and typically corresponds to a pair of reflectors, where the top is mapped in a trough and the base in a peak. Horizon interpretation from the larger amplitude volume covered around 740 km^2 and was performed using automatic and manual reflector tracking. The root mean square (RMS) amplitude map, extracted between the top and base horizons, was assessed to be the best option for analysis of seismic geomorphology since it represents the seismic response of the Marlim unit as a whole. A time versus depth conversion was performed in the larger seismic volume using a 3D velocity model calibrated by the velocity function of 38 wells (Figure 2). This process allows for the proper assessment of the thickness variations and improved seismic and well data integration. A thickness map of the Marlim unit, calibrated by wells, was calculated and filtered where the seismic horizons were mapped with high confidence, mainly in areas of moderate to high RMS amplitude values. Therefore, the map excludes areas with very low amplitudes, where the seismic mapping is uncertain and produces anomalous thickness patterns.

Several wells with standard wireline logs (gamma-ray, resistivity, density, neutron and sonic) were used to calibrate seismic response. The top and base markers of the Marlim unit consist of lithological breaks seen in cores and changes in well log patterns. The breaks are identified between low porosity (and higher density), low resistivity and high radioactivity mudstones and high porosity (and lower density), high resistivity and low radioactivity sandstones or interbedded lithologies (intercalation of mudstones and sandstones) (Figure 2). Within the Marlim unit, a simple electrofacies classification created using the density and neutron logs was used to assess lithological variability and sandstone percentage. Although gamma-ray logs have a good correspondence with the neutron and density logs, they were not used due to the arkosic composition of the sandstones. Core descriptions at the cm scale provided sedimentological information regarding facies and grain size (Figure 2). The integrated data analysis allowed the definition of architectural elements.

Strike stratigraphic sections were hung from a stratigraphic datum to (i) provide insights into the thickness and architectural changes, (ii) constrain the position of key stratigraphic surfaces and (iii) support the development of an evolutionary stratigraphic model. The stratigraphic datum was identified by a change in well log patterns within a fine-grained interval above the Marlim unit. This change is observed in all the wells and is marked by an increase in gamma-ray, neutron and transit time values and a slight decrease in the density and resistivity values (Figure 2), and possibly represents a lithological contact between a unit with higher carbonate content and a predominantly siliciclastic interval. The carbonate interval might be related to a higher amount of pelagic sediment, marking a condensed section.

4 | RESULTS

4.1 | Marlim unit geological setting

The Marlim unit is a buried sand-prone submarine slope system, 14 km wide and 40 km long, which deepens southeastward below the modern Campos Basin slope, forming the most prominent sand-prone package in the study area (Figure 3). At the time of the Marlim unit deposition, the Campos Basin had evolved into passive margin physiography, with a well-defined continental shelf, slope and basin floor (De Gasperi & Catuneanu, 2014). Like other Oligocene and Miocene

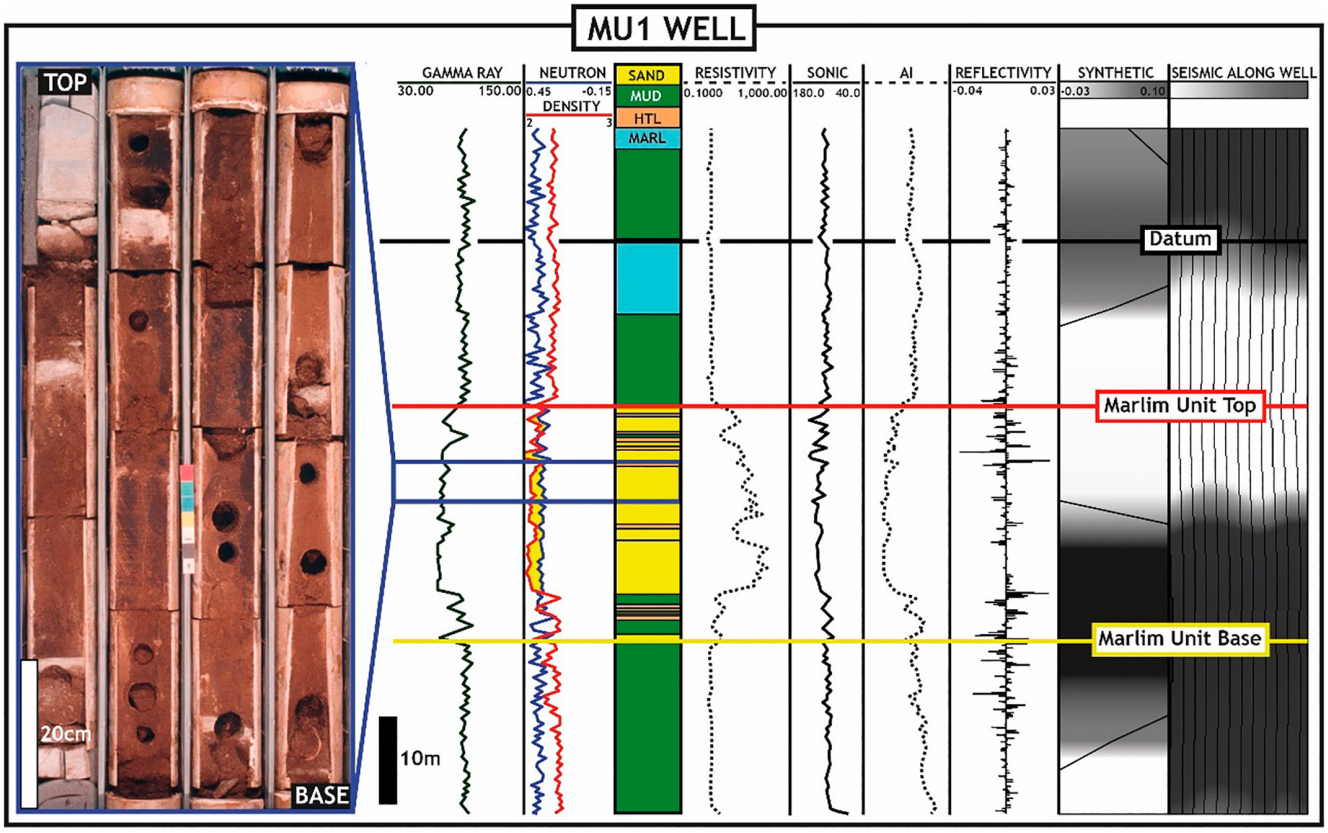

FIGURE 2 Example of well logs characteristics of the Marlim unit and the datum used (see text for explanation). The lithology log shows three electrofacies (sandstone in yellow, mudstone in green and heterolithics in pale orange). The light blue package marks the higher carbonate content interval used as a stratigraphic datum. The dark blue box represents an example of a cored interval (fine-grained structured sandstones). The Marlim unit's seismic expression is mostly a single seismic loop (trough + peak). It can be seen in the synthetic seismogram (top marked in a trough and base in a peak) that fits with the seismic log extracted in the well trajectory showing the adjustment made by the time versus depth conversion. Units: API (American Petroleum Institute) for gamma-ray, g/cm^3 for density, porosity units for neutron, ohm/m for resistivity, ms/ft for sonic, kPa s/m for AI (acoustic impedance). Other wells will be presented in the same units.

deep-water sandstones of the Campos Basin, the Marlim unit is arkosic and fine-grained, reflecting a sediment source area landward of wide coastal plains (Fetter et al., 2009). The relatively young age and high impedance contrast between the sand-prone Marlim unit and the bounding fine-grained deposits favour the extraction of high-quality seismic images. Amplitude maps reveal distinctive geomorphological patterns in two depositional domains. The up-dip domain is characterised by moderate- to high-amplitude patchy to lobate anomalies, truncated by low-amplitude elongate anomalies, and high-amplitude elongate anomalies. These elongate anomalies are interpreted here as mud-filled channels and sand-filled channel complexes, respectively (Figure 3; see Section 4.2 for detail). In contrast, the down-dip domain comprises moderate- to high-amplitude lobate features truncated by high-amplitude elongate anomalies, interpreted as channel forms (Figure 3; see Section 4.3). These two domains are linked by a reduced amplitude transition zone (TZ, Figure 3).

Salt tectonics has played a key role in the regional stratigraphic architecture across the Campos Basin palaeoslope (e.g., Albertão et al., 2011; Cainelli & Mohriak, 1999; Guardado et al., 2000; Winter et al., 2007). The long-term impact of halokinesis in the basin supports the investigation of its effects on sedimentary processes during the evolution of the Marlim unit. Normal faults, which can be listric and/or have an associated lateral component are common in the study area. Divergent reflector patterns indicate stratal thickness increases towards fault planes active during post-salt sedimentation, including the Marlim unit (Figure 4c). Many of these faults bound the Albian-Cenomanian carbonate blocks, or rafts, fragmented during the raft tectonics, a process described as an extreme thin-skinned extension of overburden over a detachment surface above salt (e.g., Duval et al., 1992; Jackson & Hudec, 2017) (Figure 4a,c). Raft tectonics generated syn-tectonic lows and eventually troughs that were healed by siliciclastic Upper Cretaceous sediments, a process commonly described in the Campos Basin (e.g., Jackson & Hudec, 2017; Moraes et al., 2007). The areas where

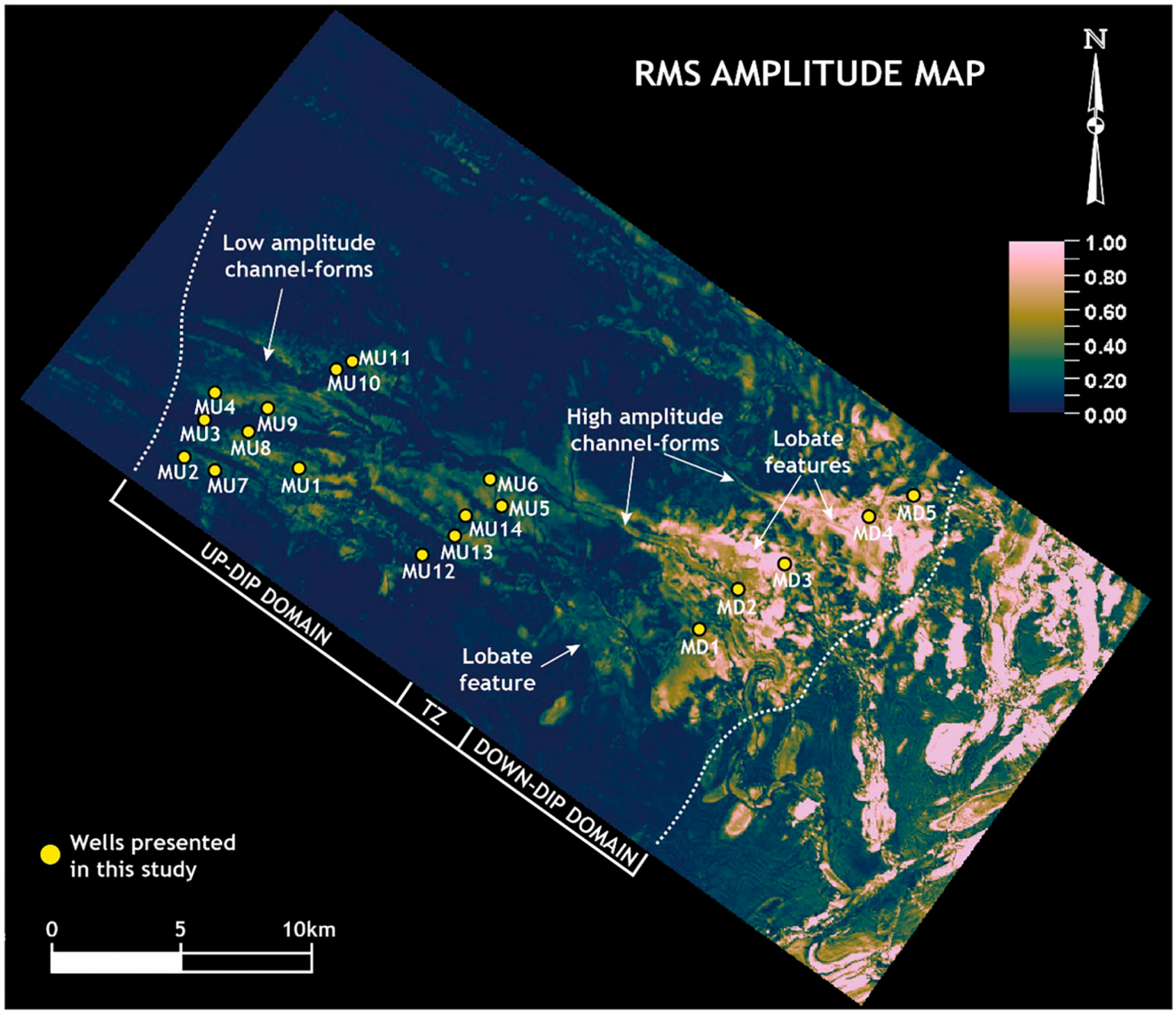

FIGURE 3 Root mean square amplitude map extracted between the top and base of the Marlim unit. Up-dip and down-dip domains show distinct seismic geomorphological responses and are connected by a transition zone. Up-dip, the seismic geomorphology suggests elongate high- to moderate-amplitude anomalies truncated by linear low-amplitude channel forms, whereas the down-dip domain comprises moderate- to high-amplitude lobate features truncated by high-amplitude channel forms.

carbonate rafts occur are subject to less compaction than areas where the post-salt stratigraphic succession predominantly comprises marine mudstones. Therefore, the more rigid carbonate rafts are interpreted to induce subtle gradient variations on the slope due to differential compaction (e.g., Collier, 1991; Jackson et al., 2008; Privat et al., 2021). This effect is supported by bounding stratal thickness patterns and subtle convexity of the reflectors (Figure 4c).

The raft tectonics and subsequent fault reactivations resulted in a complex structural configuration of rafts (highs) separated by lows (graben-like areas and troughs), and salt structures (Figure 4c). In the up-dip domain, the Marlim unit was deposited partially above carbonate rafts, and partially above an area where these rafts were markedly displaced, leading to the formation of a graben-like structure bounded by curvilinear faults-orientated NW-SE and NE–SW (Figure 4). The TZ coincides with an area between two carbonate rafts, where a thick salt ridge formed, and with a structural high formed by faulting in a raft (bounded by antithetic and synthetic NE–SW trending faults). In the down-dip domain, the Marlim unit was deposited in part above the flanks of carbonate rafts and above a zone where no major carbonate rafts are observed. Intense faulting is observed in this area and basinward, and a series of N-S to NE–SW trending normal faults (mainly synthetic) follow the orientation of salt structures, forming high displacement faulted rafts and/or prominent rollover features (Figure 4).

The isopach map shows that thicknesses are highly variable, ranging from a few metres to more than 90 m

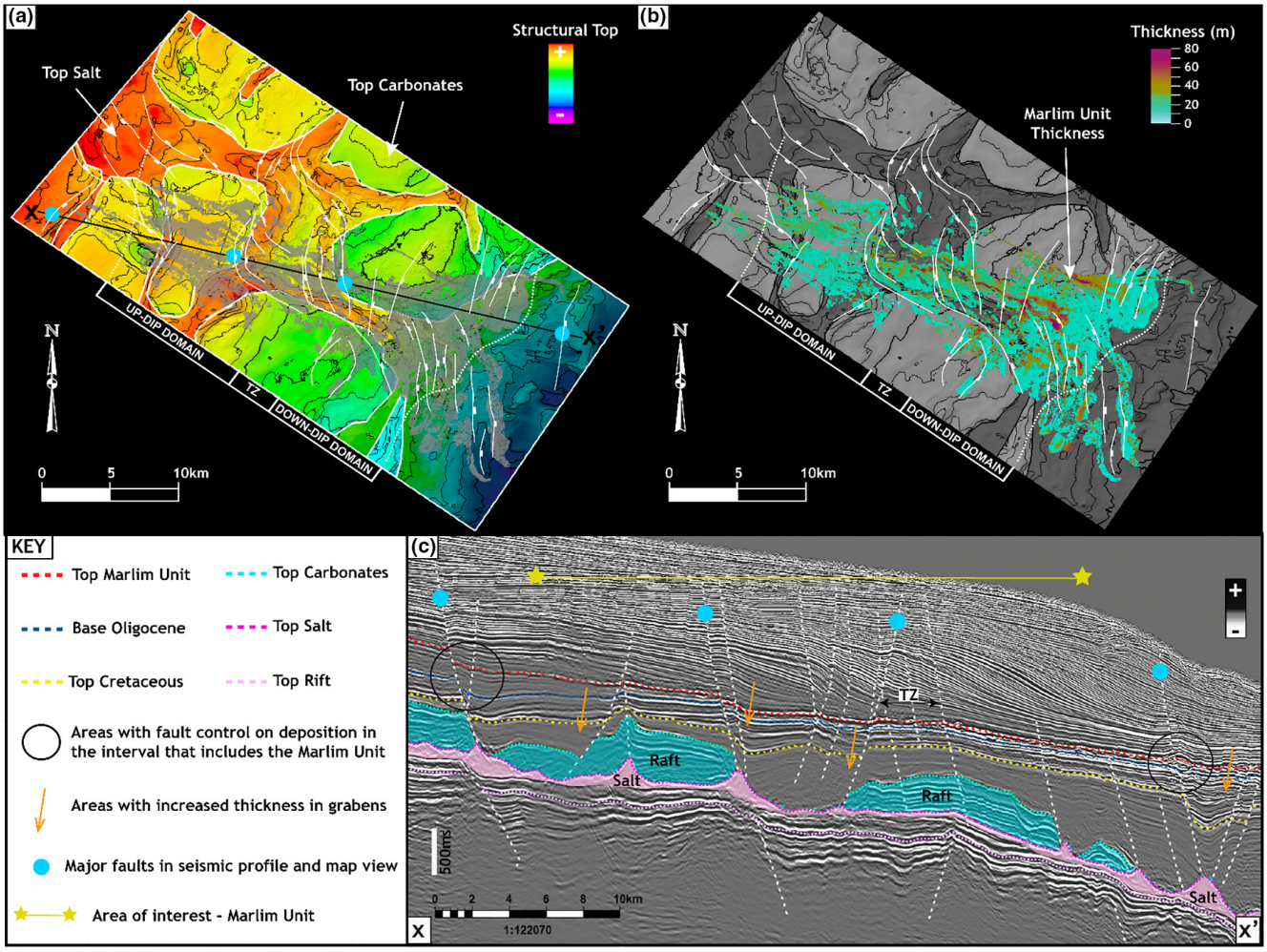

FIGURE 4 Structural configuration in the study area (fault traces at the Marlim unit level on the maps). (a) Focus on the structural tops of the salt layer and the carbonate rafts with a transparent surface of the Marlim unit displayed above; warm colours indicate higher structures and, therefore, lower depths (see text for explanation). (b) Focus on the Marlim unit thickness map displayed above grey structural tops of the salt layer and carbonates rafts. (c) Dip seismic section X-X′ (see location in (a), time domain, 5× vertical exaggeration). The orange arrows indicate areas with increased thicknesses in grabens, supporting syn-sedimentary fault activity. The black circles indicate clear fault control on deposition from the base of the Oligocene to the top of the Marlim unit in the vicinities of the area of interest marked between the two yellow stars. The carbonate rafts were displaced above the salt and control overlying thickness patterns due to differential compaction (see how the interval between the top Cretaceous and the Marlim unit thins above the rafts). The transition zone partially coincides with a relative structural high formed due to faulting in a raft. The Marlim unit is very thin in the seismic profile, and the base is interpreted in the black peak just below the top, shown as a red seismic horizon.

(Figure 4b). Average thicknesses are 22 m in the up-dip domain and 26 m in the down-dip domain, indicating that large areas of the Marlim unit are close to the vertical seismic resolution. Consequently, the seismic reflectors' character show limited variability in amplitude profiles.

4.2 | Up-dip domain architectural elements

The up-dip domain of the Marlim unit is characterised by NW-SE trending low- and high-amplitude elongate seismic anomalies, which cut seismic anomalies with patchy to lobate morphologies. Outside and up-dip of this domain is an area of overall dim amplitude anomalies without clear geomorphology, which through calibration by well data is marked by high mud content (Figure 5a,b).

4.2.1 | Low-amplitude elongate anomalies

4.2.1.1 | *Observations*

The most distinctive architectural features in the up-dip domain are parallel to sub-parallel low-amplitude elongate features with low planform sinuosity and channel-form (Figure 5a,b), which truncate underlying reflectors

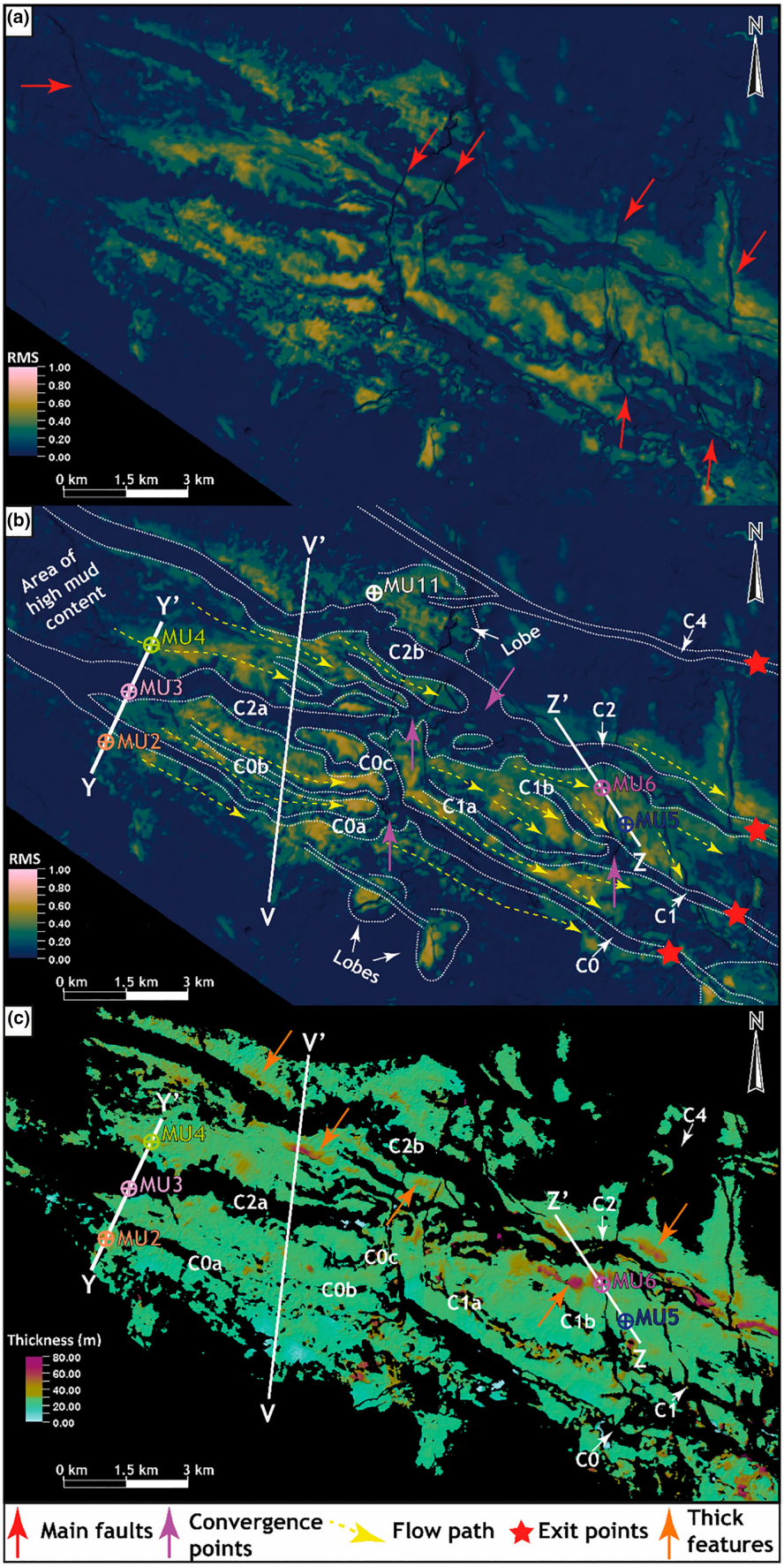

FIGURE 5 (a,b) Uninterpreted and interpreted root mean square amplitude map focused on the up-dip domain. (a) Red arrows indicate the main faults in the area. (b) Yellow arrows mark the path of high-amplitude anomalies. Dashed white lines mark geomorphological patterns of the mud-prone channel fills, which show convergence points (purple arrow) when crossing faults (red arrows). The red stars mark the exit points of the mud-prone channel fills towards the transition zone. Mud-filled channels are named C0–C2 and C4 (C3 is only down-dip) and their branches with letters a–c. Seismic profiles marked in b are shown in Figures 6 and 7. (C) Up-dip domain thickness map. Orange arrows indicate thicker elongate features interpreted as channel fills.

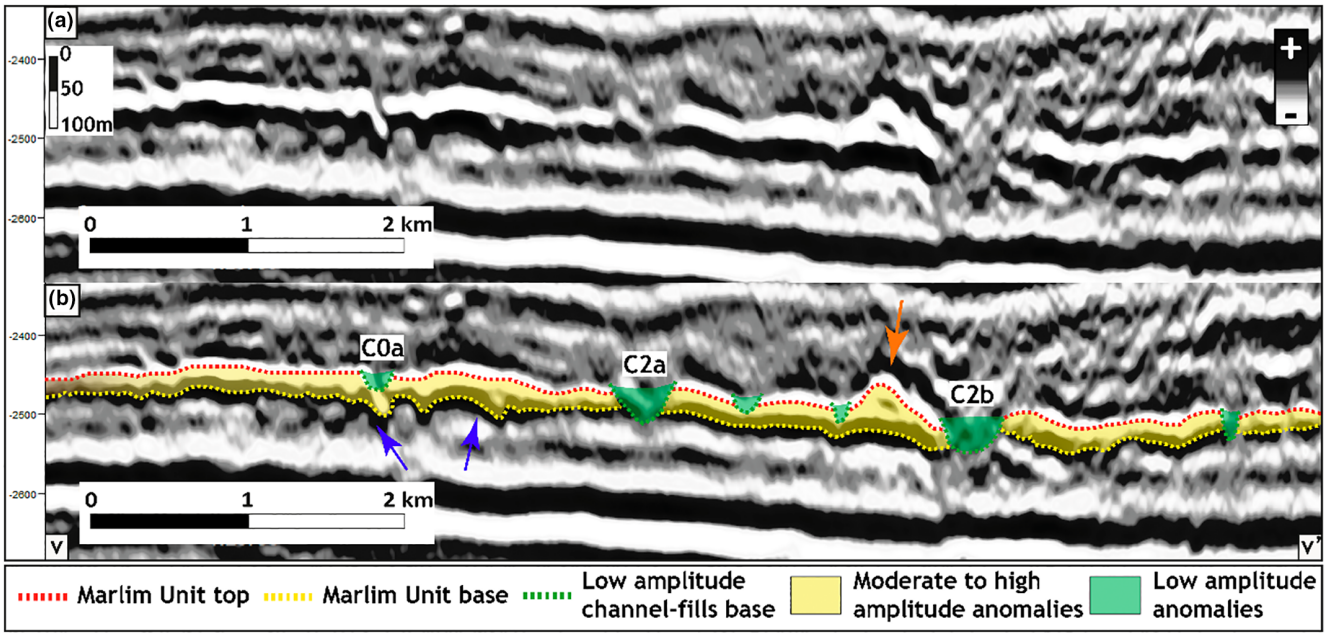

FIGURE 6 (a,b) Uninterpreted and interpreted V-V′ strike seismic amplitude profile (depth, 5× vertical exaggeration) showing the seismic expression of the Marlim unit in the up-dip domain. Note high-amplitude reflectors cut by low-amplitude channel fills and the irregular character of the base reflection suggesting basal erosion notches (blue arrows). The orange arrow indicates a feature interpreted as a transverse cut of a channel fill with positive relief due to more compaction of the finer-grained sediments that flank the channel fill axis. This feature corresponds to an elongate thicker body on the thickness map. See Figure 5 for location of seismic line.

(Figure 6). The low-amplitude features are named C0, C1, C2 and C4 (C3 is only down-dip) and range from narrow and shallow, like C0, C1 and C4 (up to 300 m wide, 30 m estimated incision depth), to wide and deep, like C2 (up to 600 m wide, 60 m estimated incision depth) (Figures 5 and 6). These channel forms display channel branches that crosscut and locally converge when crossing faults (Figure 5). Well log motifs that intersect the low-amplitude elongate channel forms are similar to the overlying stratified mudstone successions. Well intersections also support a thin (a few metres) coarser-grained basal unit (Figure 7a).

4.2.1.2 | *Interpretation*

The geometry and basal erosion of the low-amplitude elongate anomalies, and the similarity to well log motifs from overlying mudstone successions, support interpretation as mud-filled submarine channel fills. The coarse basal unit represents a sediment bypass-dominated phase of channel development. The mud-filled channels C0, C1, C2 and C4 exit the up-dip domain and pass across the TZ in four different locations (Figure 5b). The lengthening of the mud-filled channels across the TZ suggests a connection with the down-dip domain.

4.2.2 | High-amplitude elongate anomalies

4.2.2.1 | *Observations*

The RMS map shows moderate- to high-amplitude elongate anomalies that form flat- to irregular-based and continuous to semi-continuous reflectors in seismic profiles, which truncate underlying reflectors, and which are themselves cut by the mud-filled channels (Figures 5–7). Locally, these reflectors thicken in seismic profiles and correspond to thicker elongate (>50 m thick) features in the thickness map (Figures 5c, 6 and 7b). Well log motifs (gamma-ray, density and neutron) are variable. Well calibration indicates moderate to high sandstone percentage (average 58%) for these moderate- to high-amplitude reflectors. Cores display limited grain size variation, and fine-grained structured sandstones dominate the sandier packages (Figure 7b).

4.2.2.2 | *Interpretation*

Observations of the planform morphology of individual thicker moderate- to high-amplitude seismic anomalies with basal truncation support the interpretation of the moderate- to high-amplitude elongate anomalies as submarine channel complexes. Flat to irregular-based high-amplitude reflectors are attributed to laterally stacked sand-prone channel fills. Similar seismic responses have been associated with amalgamated channel complexes (e.g., Jackson et al., 2008; Kane et al., 2010; Li et al., 2021). External levees are not identified in seismic profiles or well data. Therefore, the channel complexes are interpreted to be confined through erosion and degradation of the slope profile. The channel complex interpretation is further supported by the well log motifs and sedimentary facies that indicate sand-, and intercalated sand and mud fills. Local amplitude decreases

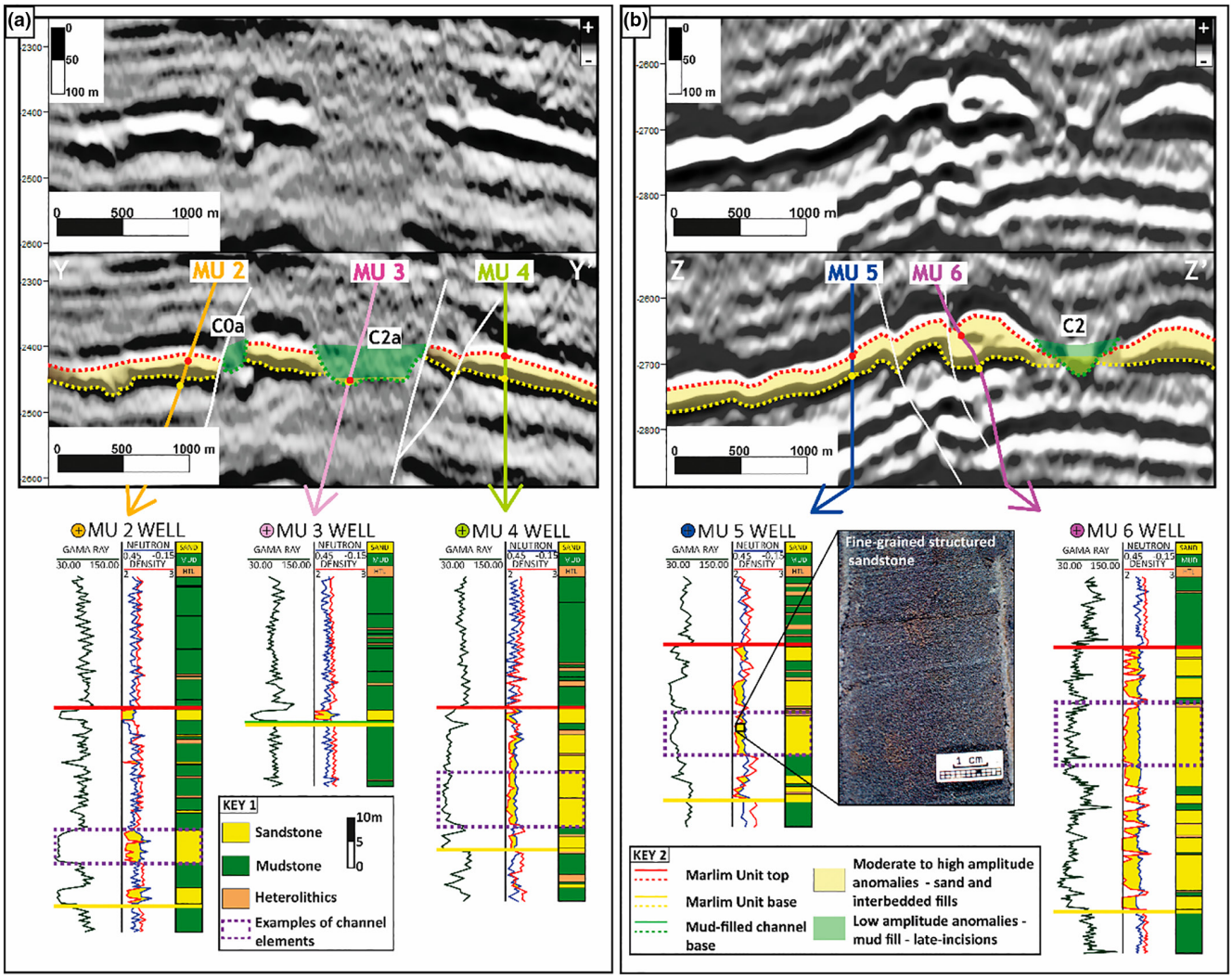

FIGURE 7 (a) Y-Y′ detailed strike seismic amplitude profile (depth, 5× vertical exaggeration) with three well intersections. MU2—example of heterogeneous and laterally stacked channel fills. MU3—well intersecting mud-prone channel fill. MU4—example of sand-prone channel fill. (b) Z-Z' detailed strike seismic profile (depth, 5× vertical exaggeration) with two well intersections. MU5—cored well with fine-grained structured sandstones. MU6—example of a sand-prone channel fill intersecting a high thickness feature in the seismic profile (with scale compatible with a perpendicular section of a submarine channel) seen on the thickness map as an elongate thicker body. Basal truncation is suggested by the reflector's patterns. See Figure 5 for location of seismic lines.

correlate to the intercalation of sandstone and mudstone packages, which support the interpretation of channel margin deposits (e.g., Hodgson et al., 2011) of laterally stacked channel fills (Figure 7a).

4.2.3 | Moderate- to high-amplitude patchy to lobate anomalies

4.2.3.1 | *Observations*

Moderate- to high-amplitude anomalies form indistinct patchy morphologies due to truncation by the mud- and sand-filled submarine channels. Moderate- to high-amplitude anomalies also form lobate features at the SW and NE edges of the up-dip domain (Figure 5b). A cored well (MU11) that intersects a small lobate seismic anomaly at the NE edge of the up-dip domain (Figure 5a,b) records interbedded intervals composed of clean and laminated sandstone and bioturbated sandy mudstone facies, suggesting hybrid beds.

4.2.3.2 | *Interpretation*

The patchy moderate- to high-amplitude anomalies truncated by the submarine channels are likely sand-prone, but we cannot distinguish whether these are remnant channel fills or lobes or a combination. The cored well (MU11) that records hybrid beds suggest the presence of intra-slope lobes (e.g., Haughton et al., 2009; Hodgson, 2009; Kane et al., 2017; Southern et al., 2017), which were better preserved at the SW and NE edges of the up-dip domain. It is important to note, however, that parts of the up-dip domain are close to the limits of seismic resolution and were eroded by flows that carved

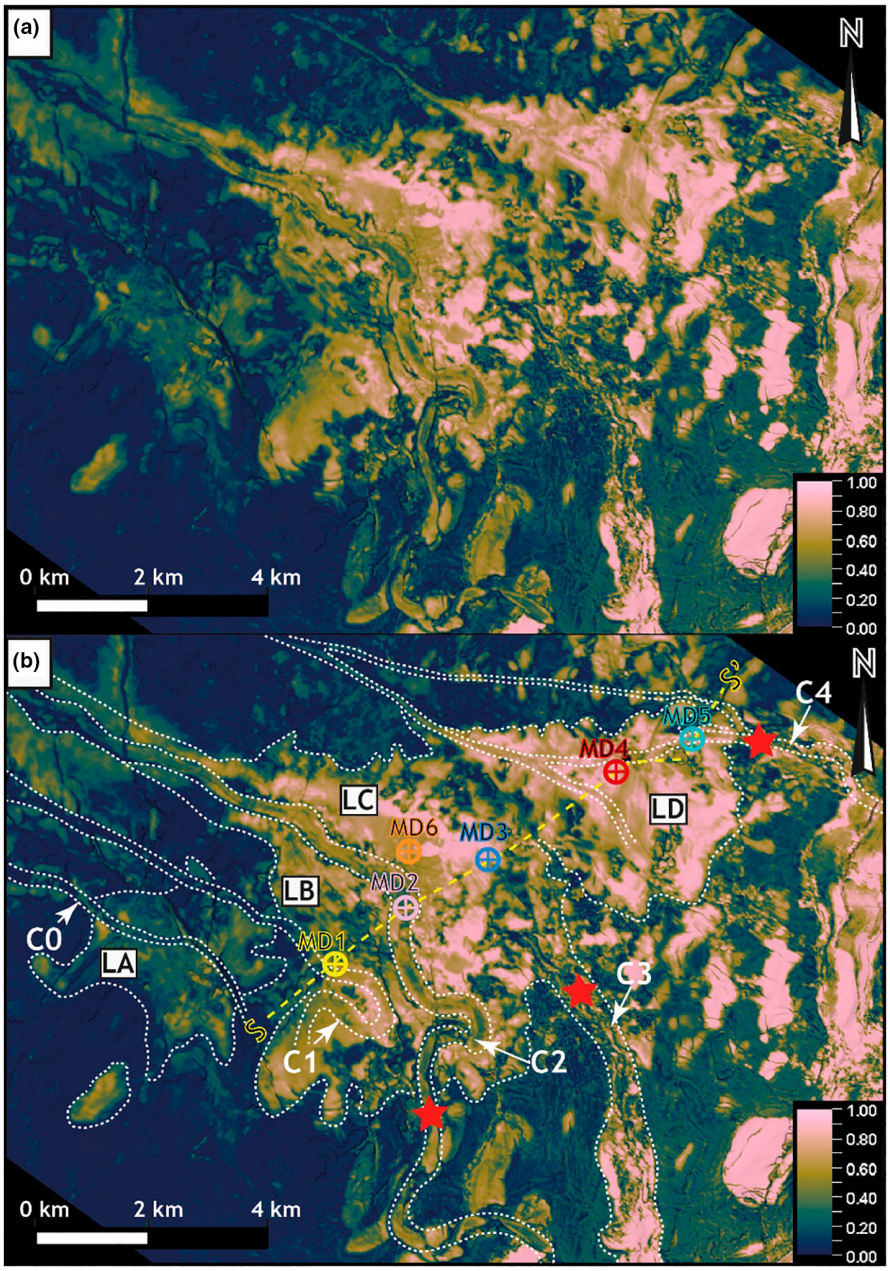

FIGURE 8 Marlim unit root mean square amplitude map focusing on the down-dip domain. (a) Uninterpreted. (b) Interpreted, with white dashed lines marking the lobate features (LA to LD) and the channel incisions, which are also indicated by the white arrows (C0–C4). The red stars mark points where the channels extend beyond the down-dip domain. S-S′ section and wells are shown in Figure 9.

the channels, subsequently filled with mud. Therefore, we recognize that some of the elongate seismic patterns might be misleading and that remnant lobe deposits might be more widely preserved across the up-dip domain.

4.3 | Down-dip domain architectural elements

4.3.1 | Moderate- to high-amplitude lobate anomalies

4.3.1.1 | *Observations*

Four lobate features characterised by moderate- to high-amplitudes are identified in the down-dip domain (named LA, LB, LC and LD) (Figure 8). The features range in area from 10 to 20 km^2. Seismic profiles and attribute maps reveal that they are connected to, and are cut by, high-amplitude elongate anomalies that connect to channel fills C0, C1, C2 and C4 from the up-dip domain. Well data and seismic amplitudes indicate that these channels, in the down-dip domain, have a sand-prone infill (Figures 3, 8 and 9), except for channel C0, which remains mud-filled above feature LA. The sand-prone channel fill C1 cuts feature LB; C2 cuts features LC and LD; C3 emerges between features LC and LD; and C4 cuts feature LD (Figure 8). Logs from wells that intersect channels C2 and C4 reveal a blocky pattern, suggesting highly amalgamated sandstone beds (Figure 9). A continuous cored interval from two wells that intersect C2 confirms amalgamated moderately

sorted, fine- to medium-grained structureless sandstones, with coarse sand (<5%). A fine-grained interval <10 m thick, composed of bioturbated siltstone with well-preserved trace fossils (*Zoophycus*) is observed with sharp contacts within the sand-prone packages towards the top of the fill of channel C2 (Figure 9). Calibration with well logs suggests that this siltstone interval is present in the eight wells that intersect channel C2.

Compared to the mud-filled channels, the sand-prone counterparts are wider with higher sinuosity (see channels C1 and C2; Figure 8). Channel C4 also widens and branches (Figure 8). Channel C3 forms a partially preserved high-amplitude feature that converges down-dip of LC and LD towards channel C2 (Figure 8). Channels C2, C3 and C4 are mapped to exit the down-dip domain in different locations and to extend basinward (Figure 8).

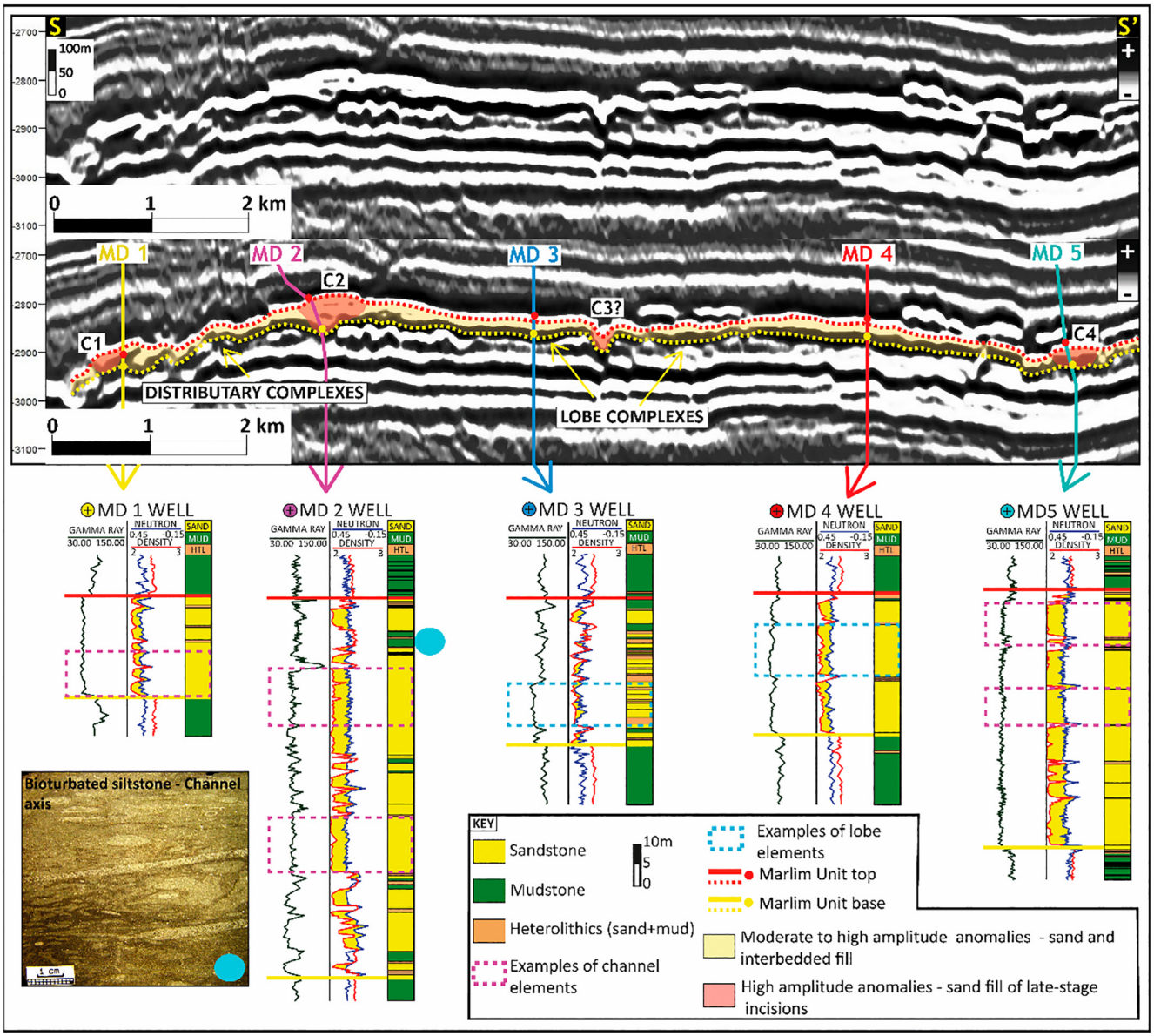

FIGURE 9 S-S′ strike seismic amplitude profile (depth, 5× vertical exaggeration) crossing LB, LC and LD features with five well intersections. Reflector's continuity and truncation differentiate distributary channel complexes from lobe complexes (see text for explanation). Blocky well log motifs are common and highlight the high sandstone percentage in the area. Examples of architectural elements' log response are marked on the wells. The MD1 well intersects distributary channel complexes deposits. The MD2 and MD5 wells intersect the axes of thick late-stage incisions channel fills (C2 and C4, respectively). The MD3 well shows a moderate sandstone percentage in interbedded successions found at the marginal positions of lobes, whereas high sandstone percentage shown by the MD4 well relates to central positions. Core of the bioturbated siltstone interval was recorded within the sand-prone axis deposits of channel C2 (see text for explanation). See Figure 8 for location of the seismic profile.

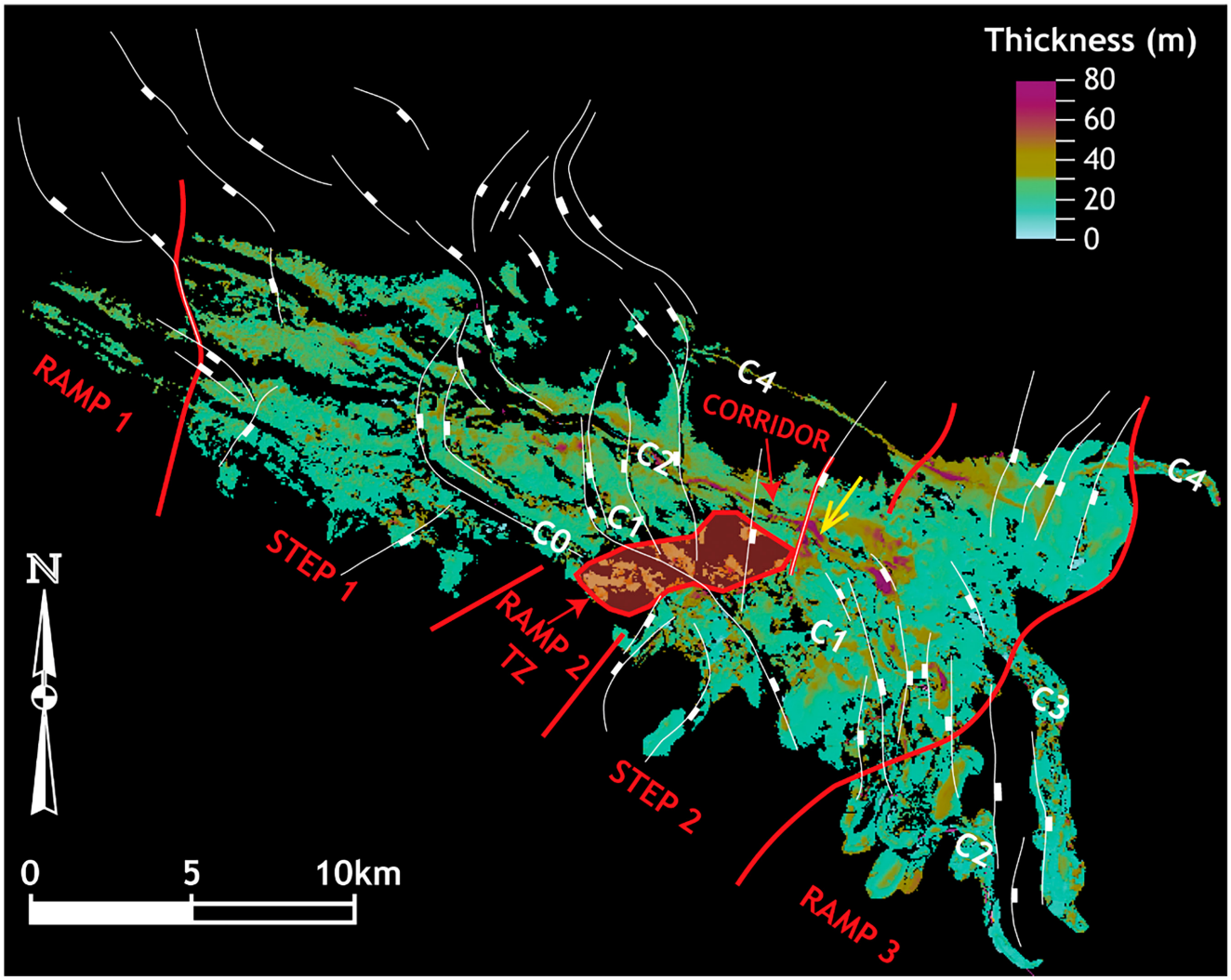

FIGURE 10 Marlim unit structural and thickness map with the location of the slope breaks (marked by red lines) and slope sectors. The up-dip and down-dip domains are interpreted as steps edged by high-gradient ramps (the transition zone includes a ramp and a corridor). Note that some slope breaks coincide with faults. Channels C0–C4 are marked. See the increased thickness recorded at the slope break of step 2 (yellow arrow, features LB and LC and C2) and the general trend of thickness increase from the south-west towards the north-east.

Well data indicate that a high sandstone percentage characterises lobate features LB, LC and LD (75% on average). Many wells that intersect different seismic facies display blocky gamma-ray and density-neutron log signatures, interpreted as an amalgamation of porous sandstone packages (higher porosity as the separation between density and neutron logs increases) (Figure 9). Therefore, the architectural interpretation is based on reflector characteristics combined with log patterns. High-amplitude, continuous to semi-continuous and tabular to mounded reflectors are recognised in features LC and LD. In contrast, moderate- to high-amplitude, discontinuous and irregular-based reflectors are present in LA and LB. The edges of features LB, LC and LD present a moderate sandstone percentage (ca. 50%) with the intercalation of sandstone and mudstone beds (well MD-3 in feature LC, Figure 9). Lithology data are not available in feature LA. In general, there is a thickness reduction from the feeder point towards the distal parts of features LC and LD, although wells show moderate thicknesses (around 20 m thick) in these distal areas (Figure 9), and amplitude continuity suggests a well-defined sand pinch-out (features LB, LC and LD, Figure 8). A cored well intersecting the central part of feature LC displays well-sorted fine-grained structureless and structured sandstones (well MD6, Figure 8b).

4.3.1.2 | *Interpretation*

Continuous to semi-continuous bright amplitude reflections with fan-shape morphology have been frequently associated with stacked lobes in intra-slope settings (e.g., Adeogba et al., 2005; Deptuck et al., 2012; Howlett

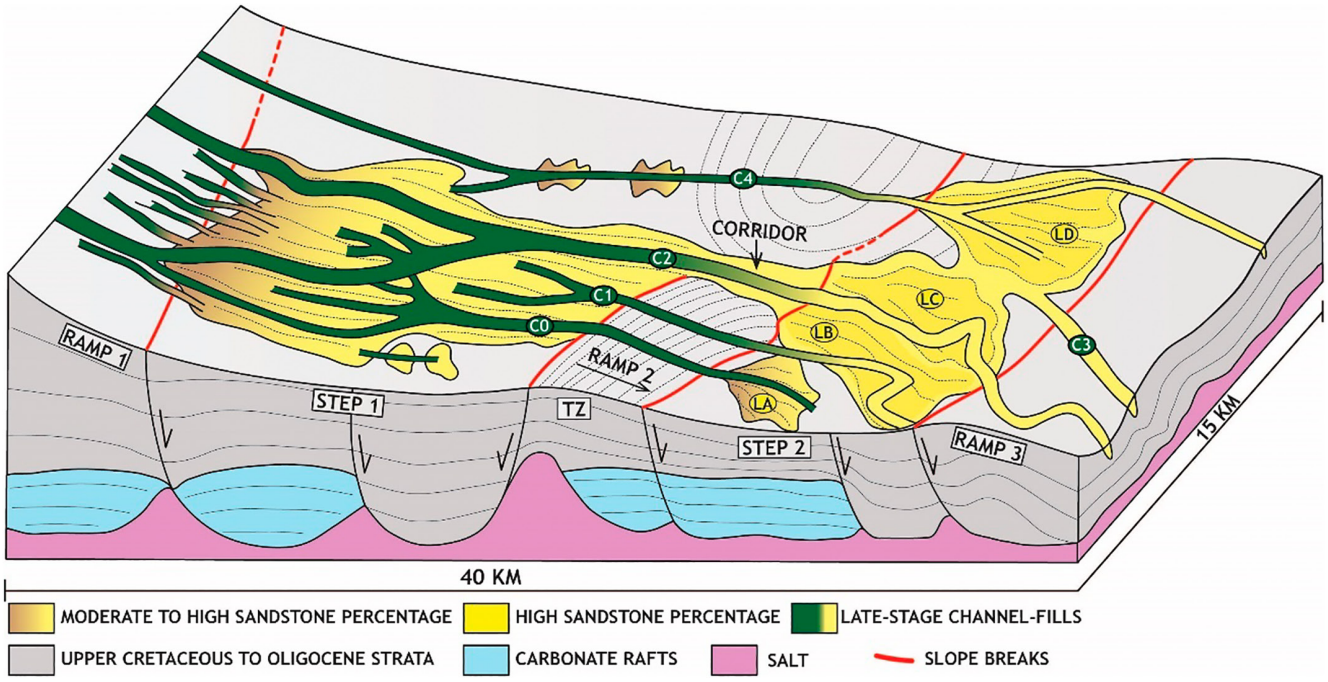

FIGURE 11 Large-scale topographic configuration of the stepped slope representing a static view of the seafloor at the end of the Marlim unit deposition. Steps 1 and 2 form two stratigraphically linked depocentres that record channel and lobe complexes (see text for explanation).

et al., 2021; Jackson et al., 2008; Jobe et al., 2017; Li et al., 2021). On the other hand, discontinuous high- to moderate-amplitude reflectors have been related to distributary channel networks (e.g., Hay, 2012) and channel complexes (e.g., Barton, 2012; Kane et al., 2012). Blocky wireline log responses (low gamma-ray values, low-density values and low neutron reading) that reflect amalgamated sandstone beds have been associated with channels (e.g., Chima et al., 2019; De Gasperi & Catuneanu, 2014; Kane et al., 2012) and lobes axes (e.g., Prather et al., 1998; Steventon et al., 2021). Intra-slope lobes or fans are described as having relatively high sand content towards the fringes and well-defined sand pinch-outs, differing from the fringes of basin floor lobes that can be quite mud-prone, thin and with poorly defined pinch-outs (e.g., Jobe et al., 2017; Spychala et al., 2015). Therefore, the seismic facies and geomorphology of features LC and LD are consistent with an interpretation of intra-slope lobe complexes. In contrast, the external planform morphology of features LA and LB suggests relatively unconfined deposits, but the seismic reflector characteristics suggest channelised elements. The arrangement of these elements in planform amplitude patterns is inconclusive as the amplitude response is affected by faulting and reservoir fluids (oil vs water contact). However, due to the lobate external shape, we interpret features LA and LB as distributary channel complexes. The high sandstone percentage observed in feature LB suggests amalgamated channels, whereas the seismic character suggests higher lithological variability in LA.

4.4 | Topographic configuration and control of the Marlim unit

The large-scale topographic configuration of the slope during the evolution of the Marlim unit is interpreted from the seismic architecture and lithological attributes described above (Figures 10 and 11). In addition, some control is invoked through correlation with the spatial distribution of underlying salt structures, carbonate rafts and associated faults (Figure 11). The seismic reflection data show no evidence for down-dip sills or three-dimensional closure, and the cores show no sign of flow ponding, such as turbidites with thicker normally graded mud caps.

The up-dip and down-dip domains are depocentres with multiple channels that cut lobes, separated and bounded by low amplitude but channelised areas (Figure 3), which support the presence of a stepped slope profile. The two depocentres represent up-dip (step 1) and down-dip (step 2) steps (Figures 10 and 11). Up-dip of step 1, irregular and low-amplitude anomalies and the dominantly mud-prone character of the deposits indicate a propensity for sediment bypass and lower preservation potential for sand, suggesting deposition in a higher gradient sector of the slope (ramp 1—a bypass-dominated zone sensu Stevenson et al., 2015). The slope break from ramp

1 to step 1 partially coincides with a synthetic NW-SE salt-rooted normal fault that edges a carbonate raft (Figure 10).

The TZ between steps 1 and 2 comprises two distinct elements: an area of weak to moderate amplitudes, which is laterally associated with a high-amplitude and sand-prone narrow elongate feature (Figures 3, 10 and 11). The low-amplitude area supports high mud content and low preservation for sand. Therefore, we interpret this area as a high-gradient ramp that allowed flows to bypass and connect the steps. The channels that feed and cut the lobate features LA and LB down-dip support this configuration (Figures 10 and 11). In contrast, the high-amplitude narrow zone is interpreted as a corridor above the lateral flank of a carbonate raft, where flows converged and connected steps 1 and 2. This corridor formed between the higher gradient ramp and a positive topographic feature that possibly originated from differential compaction above the apex of the same raft (Figure 11), as supported by thinner strata towards the centre of the structure.

The lobate features of step 2 formed above the down-dip flanks of carbonate rafts towards an area without major underlying rafts. Feature LC and parts of LB form at the exit of the corridor, down-dip of a slope break that coincides with an SW–NE synthetic fault that forms a structural high that was orientated transverse to flows (Figure 10). Increased thickness of the lobes and channel fill (C2) adjacent to the fault plane support that this structure was an active feature during deposition (Figure 10, yellow arrow). The slope break of feature LD is not associated with any resolvable structure, although differential compaction at the flanks of the carbonate raft underlying LD could have impacted the palaeoslope configuration. Down-dip of step 2, channels C2, C3 and C4 extend basinward as isolated features, and there is no significant sand deposition associated with the Marlim unit outside of these channels. We interpret that these channels evolved in a steeper sector of the slope compared to steps 1 and 2. Thinning of Cenozoic strata above rollover anticlines and faulted blocks associated with salt-rooted listric normal faults suggests the presence of irregular bathymetric features down-dip of step 2. Despite the observed lateral variability in expression, we refer to this area as ramp 3.

The contrasting depositional characteristics observed on steps 1 and 2 (architecture, thickness patterns and sandstone percentage) suggest differences in the geometry of the associated slope breaks and accommodation on the steps. The sand-prone lobe complexes documented in features LC and LD above step 2 support an abrupt slope break, which led flows to lose their capacity to transport coarser fractions and induced flow expansion due to rapid loss of confinement (e.g., Mulder & Alexander, 2001; Spychala et al., 2020). The thickness increase recorded downstream of the slope break in the proximal parts of step 2 also suggests substantial gradient variations. This interpretation is supported by experimental studies that show thicker slope break deposits associated with abrupt gradient changes (e.g., Kubo, 2004; Mulder & Alexander, 2001). Conversely, a milder slope break, between ramp 1 and step 1 and in features LA and LB, would permit flows to remain channelised. Channel stability across mild slope breaks has been documented in channels in intra-slope basins described by Booth et al. (2003) and Barton (2012).

In summary, the geomorphological patterns of the Marlim unit point to a complex palaeoslope topography comprising alternating depositional (steps) and bypass-prone areas (ramps), with breaks-in-slope of variable magnitude and physiography that are related to underlying salt-related tectonic features (Figure 11). The presence of multiple mud- and sand-filled channels that connect the steps across the ramps (Figures 5, 8 and 11) suggests multiple non-synchronous sediment conduits. Gradient variations imposed by slope breaks along channel profiles were probably readjusted via up-dip migrating knickpoints based on observations from modern and ancient systems (Allen et al., 2022; Deptuck et al., 2012; Guiastrennec-Faugas et al., 2021; Heijnen et al., 2020; Tek et al., 2021). The age relationship between the late-stage channels and the step deposits requires a high-resolution stratigraphic framework, which is discussed in the next section.

4.5 | Stratigraphic framework

Stratigraphic relationships observed in seismic reflection data support interpretations of key surfaces and the relative age of deposits. The up-dip submarine channel complexes in step 1 form an 8–10 km wide zone composed mainly of laterally stacked channel fills that are cut by the mud-filled channels C0, C1, C2 and C4 (Figures 5–7). The same configuration is documented in step 2, where these channel fills are sand-prone (except C0) and cut the lobate features (Figures 8 and 9). These observations support late-stage channel lengthening and incision of sand-prone deposits.

More detailed stratigraphic age relationships were observed in step 2, where the nature of the depositional system (i.e., unconfined deposition) implies an overall higher preservation potential compared to the channel complexes of step 1. The irregular and sharp external shape of feature LA suggests that it was partially eroded. It is interpreted that the erosion, at least in part, is due to truncation by channel C1, the late-stage channel interpreted to have fed feature LB. In addition, LA is surrounded by LB, which formed in a space not occupied by LA (Figure 8). These observations support LA being older than LB. The age relationship

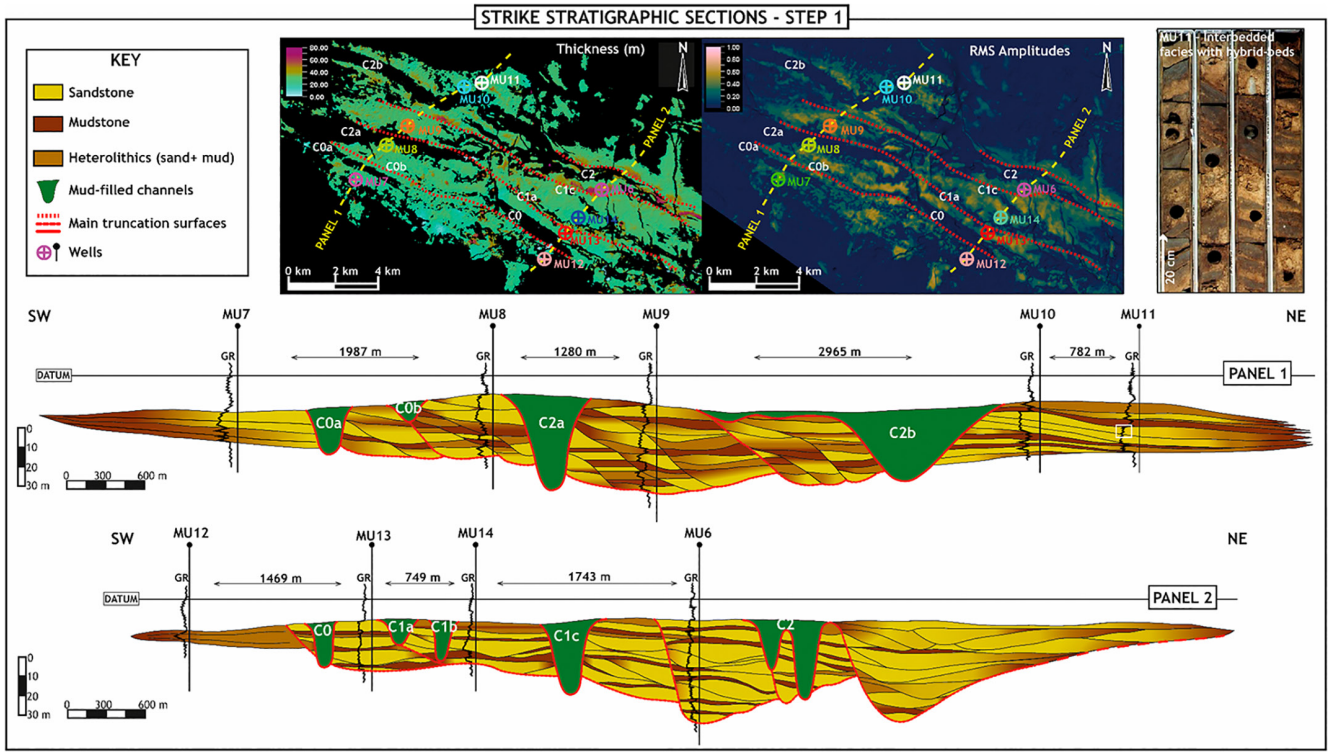

FIGURE 12 Interpreted strike panels that summarise the stratigraphic framework of step 1. Note the thickness increase trend towards north-east calibrated by wells. C0 (a,b), C1 (a–c) and C2 (a,b) represent the mud-filled channels that cut the sand-prone channel complexes and, eventually, older lobes. The red lines depict truncation surfaces. The red truncation surfaces related to the sand-prone channel fills are depicted in the thickness and amplitude maps and are interpreted in areas with abrupt thicknesses variations and/or amplitudes reduction. The black lines that limit internal architectural elements follow well logs breaks, however, their geometry is not resolved by seismic and, therefore, is speculative. Lobes are interpreted on both edges of panel 1 and at the SW edge of panel 2.

between LB and LC is not clear, and their relative position does not favour any interpretation in this sense. However, these features present distinct internal architecture and apparently have different feeder channels, supporting two depositional phases (Figures 8 and 9). C2 cuts between the two features, supporting that it is younger than LB and LC. A more compelling age relationship is observed between LC and LD. LD shows a classical lobate geometry, meaning that the feature is well preserved. On the contrary, the NE edge of LC suggests truncation by a channel (Figure 8). This could be C3; however, there is not sufficient seismic resolution to map C3 in this area. Also, the relative position between both features supports the progradation of the system since C4, the LD feeder channel, lengthened further basinward before losing confinement (compared to LB and LC). In summary, the geomorphological patterns suggest an overall oblique progradational stepping/compensational trend towards the NE, where LA is the oldest feature and LD is the youngest (Figures 3 and 8).

The stratigraphic framework of step 1 is summarised in two correlation panels orientated SW–NE, orthogonal to the channels, hung from the carbonate-prone stratigraphic datum and calibrated with nine wells (Figure 12). The correlation panels highlight the pervasive mud-filled channels, with varying widths and depths, which incise into sand-prone channel fills and lobes. Truncation surfaces within the sand-prone channel complexes are identified: (i) where abrupt reduction in amplitudes related to the edges of the elongate seismic anomalies occur, and/or (ii) in areas with abrupt and substantial thickness increase (Figure 12). We assume that lower amplitude values at the edges of high-amplitude seismic bodies can be associated with channel margin deposits that onlap onto erosion surfaces (e.g., Hodgson et al., 2011), and that abrupt differences in thicknesses in the strike direction are related to channel truncation.

Well calibration supports interpretations of lithology distribution, architectural elements and stacking patterns. Preservation of laterally stepping channel fills that comprise intercalated mud- and sand-prone packages related to channel margin deposits are common at the proximal part of step 1 (Figure 12, panel 1 wells MU8 and MU9). Homogeneous sand-prone amalgamated channel fills associated with axial deposits prevail at the distal part (Figure 12 panel 2, wells MU13 and MU6). At the SW end of the panels, wells that intersect dim seismic amplitudes suggest thin, and moderate to low sand content, and high aspect ratio geometries (Figure 12, both

panels). At the NE end of panel 1, high aspect ratio geometries intersected by two wells are depicted (wells MU10 and MU11, Figure 12). The wells show a moderate sandstone percentage (MU11 facies include hybrid beds) and were drilled in a moderate to high-amplitude anomaly without a clear elongate shape. Considering the seismic amplitude character, well data and relative position in the system, the high aspect ratio deposits are interpreted as remnant deposits of (frontal) lobes that were truncated by the channels.

Both panels reveal an overall NE-ward thickness increase, culminating in thick channel deposits of more than 40 m (41 m in well MU9, 51 m in well MU6, Figure 12). This pattern is corroborated by the thickness map (Figure 10) and suggests that accommodation progressively increased in the same direction. The panels also illustrate truncation surfaces that represent composite erosion surfaces that consistently step to the NE. The interpreted trend in lateral channel migration is supported by the depositional patterns of step 2. The physical continuity of the late-stage channels between both steps strongly suggests that these areas were stratigraphically linked during the evolution of the Marlim unit. Therefore, we interpret that the stratigraphic evolution above steps 1 and 2 share a NE-ward migration history.

We interpret that a sediment bypass-dominated period following incision occurred in the late-stage channels before they were filled with mud and/or sand (channels C0–C4). Similar channels commonly link intra-slope depocentres at the final stages of a fill-and-spill cycle, once accommodation is healed and a new down-dip base level is established (e.g., Adeogba et al., 2005; Jobe et al., 2017; Prather et al., 2012; Spychala et al., 2015). Several studies have documented bypass-dominated channels that exit intra-slope basins at a single point, in accordance with the classic fill-and-spill model (e.g., Adeogba et al., 2005; Barton, 2012; Beaubouef & Friedmann, 2000; Pirmez et al., 2000; Prather et al., 1998; Sinclair & Tomasso, 2002; Smith, 2004; Winker, 1996). In contrast, a number of studies figuratively show two or three exits, but these are inferred, as channels are either not identified through these putative exits (Meckel et al., 2002), or evidence for these has been removed by subsequent erosion (Deptuck et al., 2012). In contrast, in the Marlim unit, the bypass-dominated channels exit step 1 in four different locations and feed the lobate features of step 2. The bypass-dominated channels also exit step 2 at distinct locations (Figures 5, 8 and 11). This suggests multiple laterally associated stratigraphic cycles, each representing an episode of accommodation creation, healing and bypass in both steps (fill-and-spill cycles) and abandonment of the final channel.

5 | DISCUSSION

5.1 | The Marlim unit: Stratigraphic evolution above a dynamic stepped slope

The Marlim unit evolved above a stepped slope in an extensional salt domain, where downslope extension and salt-thinning prevailed. However, most of the extension had finished at the time of deposition, and much of the salt had flowed basinward (Quirk et al., 2012). The negative relief created by the salt-controlled raft tectonics was largely healed, implying only minor effects of salt-related deformation on the slope. Nevertheless, salt tectonics remained active and amplified by the reactivation of basement structures (Fetter, 2009). Therefore, due to the long-term trend of waning salt-related deformation, we propose a scenario where low deformation rates and subtle seafloor topography, disturbed by local fault reactivation, controlled accommodation creation in the Marlin unit slope.

The deformation style is interpreted from architectural patterns and stratigraphic relationships. The thickening direction of multiple fill-and-spill cycles to the NE, together with the persistent migration of the submarine channels and lobes in the same direction, orientated transverse to the stepped slope profile, supports syn-sedimentary lateral tilting. This contrasts with basinward tilting where submarine conduits tend to have fixed positions (e.g., Jackson et al., 2021). Without invoking a lateral tilt, the documented thickening direction and stacking pattern would need to be explained by the turbidite system initiating on the higher part of the steps (SW) and working their way progressively to lower elevations to the NE. However, turbidity currents are ground hugging and have a strong tendency to preferentially fill topographic lows through deposition (e.g., Straub et al., 2009), and therefore, this alternative scenario is considered highly unlikely.

Submarine channel systems that evolve above slopes that undergo lateral tilting can be controlled by growth faulting in extensional settings (e.g., Kane et al., 2010) or by salt dome uplift in halokinetic basins (e.g., Gee & Gawthorpe, 2006; Kane et al., 2012). In step 1, the prevalence of intercalated deposits supports the presence of laterally stepping channels with channel margin deposits preferentially preserved (e.g., Hodgson et al., 2011; Figure 12, panel 1). These channel fills are similar to channel systems that laterally migrate in response to tilting caused by halokinesis (e.g., Gee & Gawthorpe, 2006; Kane et al., 2012). However, despite the evidence for tectonic activity related to salt-cored structures in the Oligocene–Miocene interval (Figure 4), the exact cause of the lateral tilting, either uplift to the SW and/or subsidence to the

NE, is challenging to determine as no specific structural element influencing the large-scale patterns of deposition is identified. Moreover, the effects of the syn-sedimentary deformation are interpreted here at a very high-resolution scale. Although we interpret the effects, the primary cause is difficult to demonstrate in seismic reflection data, especially in a setting of low deformation rates and complex interaction between halokinesis, differential compaction and, possibly, reactivation of basement faults.

The seismic geomorphological patterns suggest four fill-and-spill cycles in both steps. The geomorphological patterns in each cycle and the stratigraphic evolution of the lateral tilting slope of step 1 are reconstructed in Figure 13. Here, accommodation is interpreted to be spatially more limited compared to step 2, which records distributary channel and lobe complexes suggestive of an area prone to sediment dispersion. Above step 1, the high propensity for erosion and bypass resulted in an incomplete stratigraphic record. The cycles are defined by the mud-filled channels and their incisional relationship with the sand-prone channel complexes and remnant lobes. Step 2 has higher preservation, and each cycle refers to one of the lobate features and associated incision (Figure 8). Less clear is the relationship between the lobate features and C3, which could have been formed during cycle 3 or cycle 4. The 'fill phase' of each cycle relates to the sand-prone deposition before the late incisions, and the 'spill phase' is associated with the bypass-dominated phase of these incisions (C0 to C4) prior to filling with mud and/or sand. After the spill phase, we interpret that the lateral tilting prevailed and drove a NE-ward shift in the location of each cycle, therefore, the cycles are here referred to as Fill-and-Spill, Tilt-and-Repeat cycles (FaSTaR). The following section will discuss the interplay between sedimentation and slope deformation within the evolutionary history of the Marlim unit.

5.2 | Intra- and extra-basinal stratigraphic controls on the Marlim unit

Slopes evolve over time depending on the interplay of substrate mobility and sediment flux (Prather, 2003), which are controlled by intra- and extra-basinal factors, respectively. The incisions identified in the FaSTaR cycles (throughgoing in three of four cycles) indicate that effective basinward sediment bypass beyond ramp 3 was repeatedly established, which suggests that a local graded profile was reached in each cycle (e.g., Adeogba et al., 2005; Deptuck et al., 2012). Therefore, we argue that the sedimentation rate outpaced the rate of lateral tilting prior to, and during,

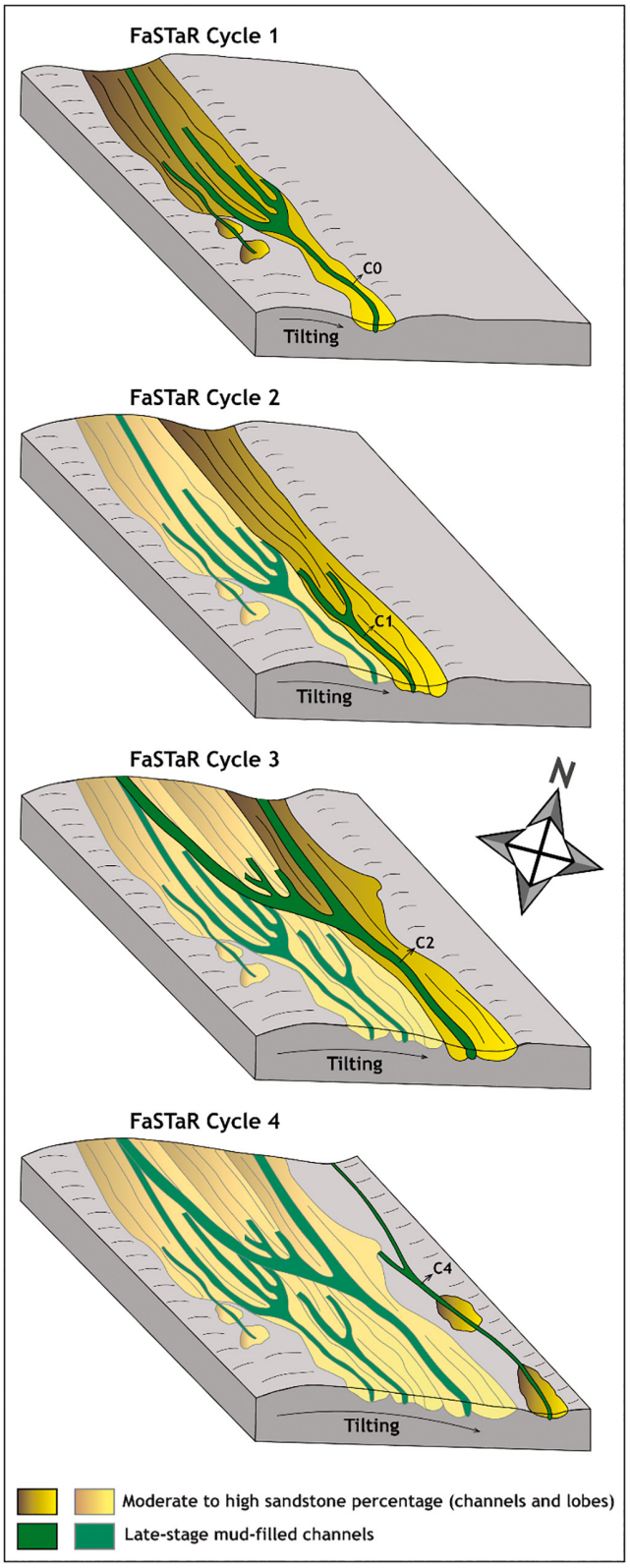

FIGURE 13 Three-dimensional diagrams that show the evolution of the Fill-and-Spill, Tilt-and-Repeat cycles on step 1 (see text for explanation). Note the thickness increase towards the north-east attributed to higher accommodation controlled by the lateral tilting (peaking at cycle 3).

these incisional periods. As outlined previously, the general structural context points to comparatively low rates of slope deformation (in this case, primarily lateral deformation) relative to the duration of the sediment supply cycles, as commonly documented in stepped slope systems (e.g., Deptuck et al., 2012; Prather, 2003). Moreover, low rates of lateral tilt are also supported by the lack of flow ponding and by the stratigraphic connection between the steps, which suggests that the axial slope dip (regional slope gradient) was more critical for sediment dispersal patterns than the lateral structural dip caused by tilting.

The record of complete cycles (i.e., healing and bypass phases) indicates that enough sediment was available to infill accommodation and bypass basinward. However, it does not necessarily indicate that the sediment supply was constant during the Marlim unit deposition. The partial filling of the late-stage channels with sandstones suggests that these channels had sand-prone flows during their lifespan. However, up-dip, the same channels are filled with stratified mudstones (analogous to the laminated and bioturbated siltstones cored in channel C2, Figure 9), here related to the settling of low-density turbidity currents and hemipelagic sediment fallout. This spatial difference in infill character of the conduits suggests an initial phase of backfilling with sands, followed by sand starvation and, ultimately, channel abandonment (e.g., Peakall, McCaffrey, & Kneller, 2000; Peakall, McCaffrey, Kneller, et al., 2000; Prather et al., 1998). This occurs repeatedly and reflects an external control on the sediment supply that resulted in discrete waxing-and-waning fill-and-spill cycles, and periods of sand starvation, when coarse clastic sedimentation was negligible but lateral tilting was active (Figure 14).

Above step 1, the sand-prone channel complexes form a composite body with overall high connectivity locally incised by the mud-filled channels. Lateral stratigraphic continuity of channel deposits above tilting surfaces results from gradual migration (combing) and has been associated with relatively low rates of tilting and/or short periods between flows, whereas pronounced stepping (avulsion) and/or isolated channel ribbons are associated with rapid tilting and/or long return periods (e.g., Kane et al., 2010, 2012; Peakall, Leeder, et al., 2000). The infill by mud in the through-going incisions suggests a long return period of the flows between the cycles. However, the overall stratigraphic signature supports low rates of tilting and, likely, a short return period of the flows during the fill-and-spill phases of each FaSTaR cycle.

The organized and predictable stratigraphic record of the sediment supply cycles suggests that accommodation was created by a continuous slow-moving tilting slope at a quasi-constant deformation rate (Figure 14) that acted as a background control, rather than being controlled by short-lived random tectonic perturbations, which would result in a less ordered record. The end of an FaSTaR cycle and the start of a new one at the end of a sand starvation period are marked by the re-routeing of the feeder channels, which we attribute to up-dip avulsions to areas with accommodation (Figure 14). The mechanism for channel avulsions can be explained by the interplay between the deformation style operating in the Marlim unit slope (intra-basinal control) and the cyclic fluctuations in the sediment supply (extra-basinal control). We speculate that the turning point for triggering avulsions could be reached once the cumulative deformation caused by the continuous lateral tilting provoked structural changes capable of altering accommodation patterns on the slope (creating a new topographic low). At the onset of a new cycle, when enough coarse sediment was again available in the system, the returning flows would interact with a substantially modified slope, with a higher potential for forming a new conduit, as also proposed by Kane et al. (2012).

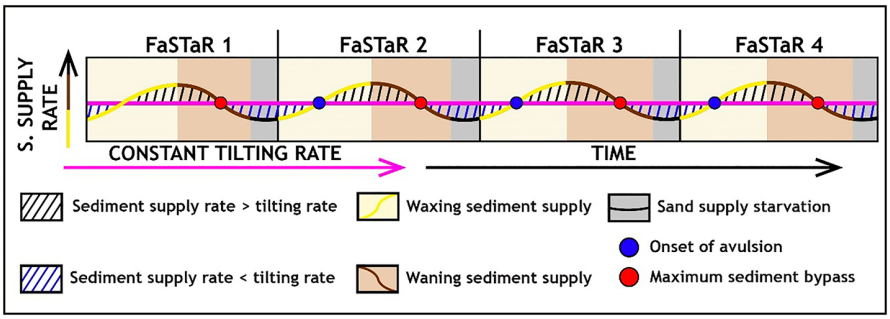

FIGURE 14 Sediment supply rate versus tilting rate in each Fill-and-Spill, Tilt-and-Repeat cycle. The cycles comprise phases of waxing and waning sediment supply and periods of sand starvation. The rate of tilting outpaces the rate of sediment supply during the end of the waning phase and the start of the waxing phase (including the sand starvation period). Conceptually, the maximum cumulative sediment bypass is positioned at the inflection point of the waning curve and the onset of avulsions at the inflection point of the waxing curve, when substantial coarse sediment is again available.

5.3 | The impact of the slope configuration on the FaSTaR cycles

Pre-existing structural elements controlled the basinward stepped profile (Figure 11). Underlying structural features such as rafts, salt rollers and associated faulting played a crucial role in the position and character of slope breaks between ramps and steps. Turbidity currents are sensitive to gradient changes and respond differently according to the magnitude and type of topographic variations (e.g., Alexander & Morris, 1994; Deptuck et al., 2012; Garcia & Parker, 1989; Kneller & McCaffrey, 1999; Kubo, 2004; Morris & Alexander, 2003; Mulder & Alexander, 2001; Stevenson et al., 2013). Therefore, the style of filling and spilling varies between each cycle according to the evolving slope configuration.

The large-scale topographic template interpreted for the Marlim unit slope (Figure 11) suggests three different slope configurations during the stratigraphic evolution (Figure 15). Cycles 1 and 2 are interpreted to have evolved in a similar topographic template comprising two steps (steps 1 and 2) and three ramps (ramps 1 to 3) (Figure 15a). In part, sedimentation in the steps evolved synchronously as there was no confining counter slope to pond sediment up-dip (Figure 15a1,a2). Ramp 1 was prone to bypass, which fed sediment through the laterally migrating channels above step 1. The channels of step 1 sourced sediments to lobate features LA and LB on step 2. Seismic geomorphology and amplitude strength indicate that lobate feature LA is smaller and less sand-prone compared to other lobate features (Figure 8), suggesting that either the flow magnitude and sand content were lower in an initial phase of the Marlim unit evolution or more sediment was bypassed basinward during this cycle. We infer that incision at the slope breaks at the down-dip edges of the steps, where a knickpoint likely formed and eroded headward to smooth the channel profile, occurred once the steps were filled to the spill point, starting from the down-dip edge of step 1, the first step to heal (Figure 15a1–a3). However, the exit point of step 2 is not clearly observed on seismic reflection data. At a final stage, a through-going channel incised cycle 1 deposits (C0) and cut through part of step 1 in cycle 2 (C1) (Figures 11 and 15a4). Later,

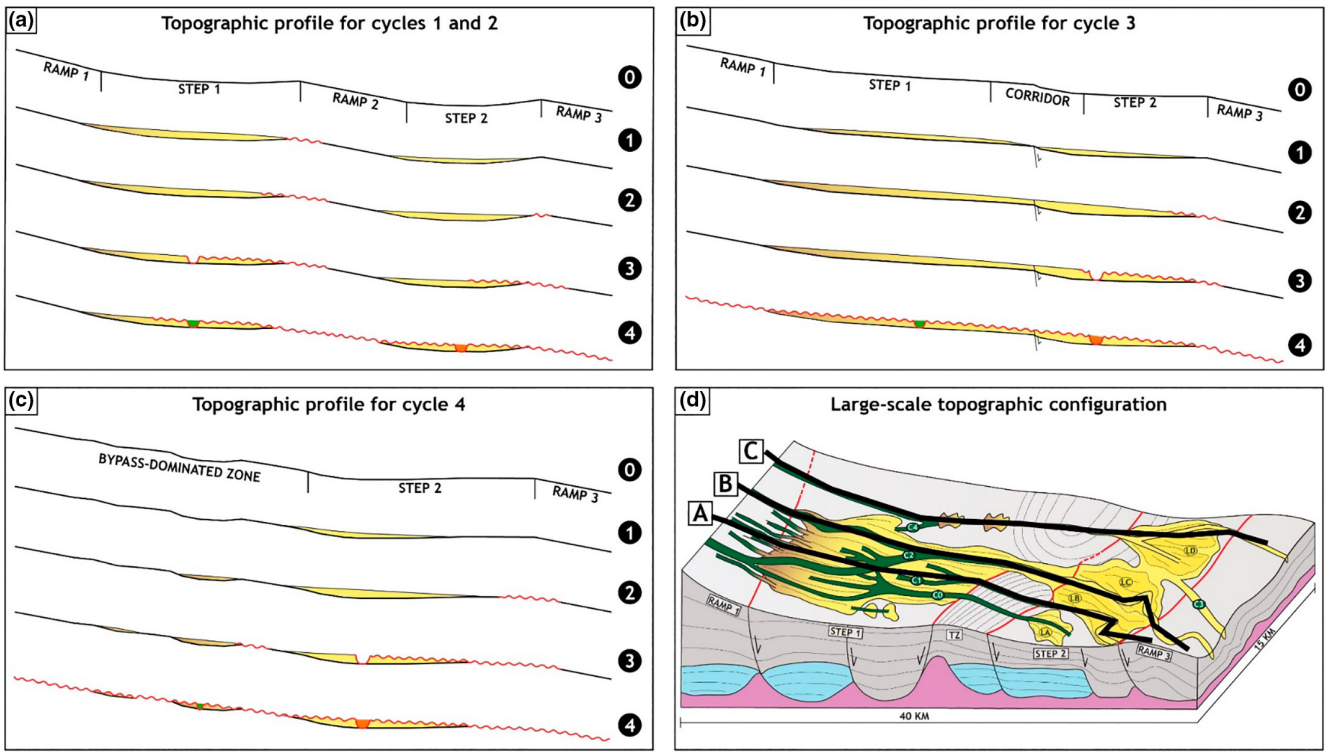

FIGURE 15 Stratigraphic evolution of each Fill-and-Spill, Tilt-and-Repeat cycle according to the palaeotopographic configuration. Time '0' represents the initial slope configuration. (a) Cycles 1 and 2 (stage 4 represents cycle 2 since in cycle 1 the incision is through-going and totally mud-filled), (b) cycle 3, (c) cycle 4. See text for detailed explanations on each cycle. (d) Location of the profiles on the topographic configuration. The profiles show the evolution of late incisions C1, C2 and C4 (red curly lines). Therefore, they are dip sections representative of where these incisions occurred. Green represents the mud filling of the late incisions, and orange represents the sand filling.

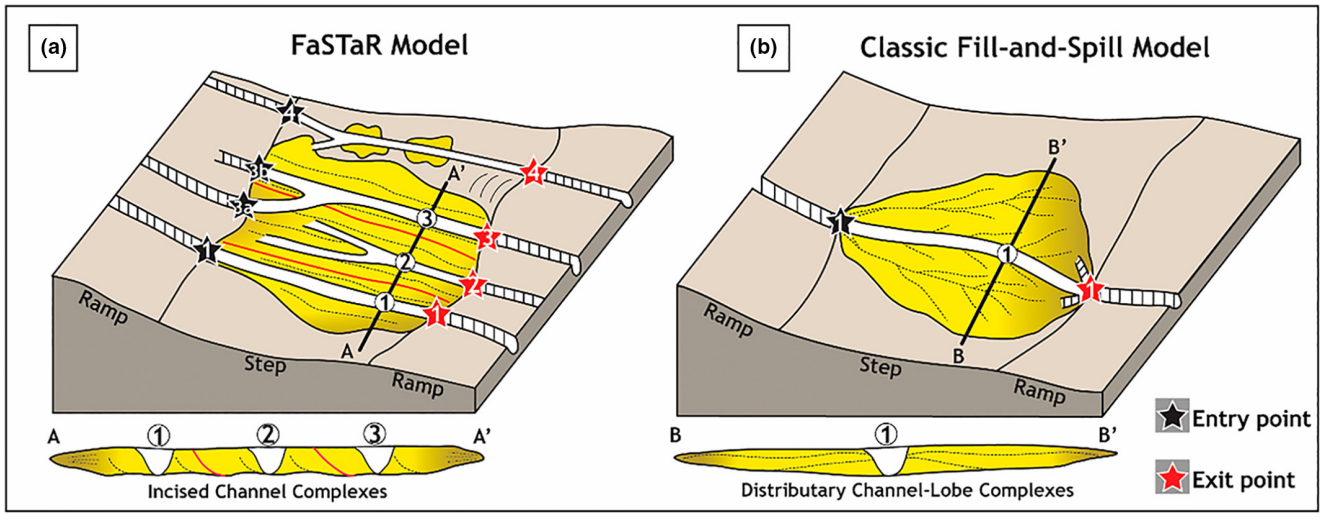

FIGURE 16 Schematic summary of the Fill-and-Spill, Tilt-and-Repeat (FaSTaR) model. (a) and the classic fill-and-spill model (b). The FaSTaR model is composed by several laterally associated cycles and multiple entry and exit points (red lines represent main truncations and limits between cycles). It contrasts with the classic model that predicts a single, or vertically stacked, cycle(s) and a single entry and exit point. The depositional architecture is also distinct. The FaSTaR cycles record incised channel complexes, whereas in the classic fill-and-spill models turbidity currents produce more unconfined deposits, such as distributary channels and lobes (see text for detailed explanation).

the conduits were filled with mud (C0) and partially with mud and sand (C1).

The slope configuration during cycle 3 differs from cycles 1 and 2 since a corridor acted to connect steps 1 and 2 in the early evolution of the cycle (Figure 15b0,b1). The topographic difference formed by the fault-controlled slope break at the corridor's exit was progressively healed (Figure 15b2). Total filling of steps 1 and 2 meant channels were able to transfer sediment across step 2 and ramp 3 (Figure 15b2) and form a through-going incision on the stepped profile (channel C2), which evolved from the down-dip edge of step 2 upwards (Figure 15b3,b4). C2 was later partially filled by sand from ramp 3 up to the distal part of step 1, and mud from step 1 towards ramp 1 (Figure 11).

During cycle 4, step 1 recorded thin, moderate to low seismic amplitude deposits in a restricted area, incised by a mud-filled channel (C4), implying limited accommodation. Therefore, the site represents a bypass-dominated zone (sensu Stevenson et al., 2015) that extends from ramp 1 to step 2 (Figure 15c0). The deposition started in step 2 by building lobate feature LD (Figure 15c1). As step 2 filled, a deep incision occurred at the edges of step 2 towards ramp 3, and deposition took place up-dip in areas with available accommodation on the bypass-dominated zone (Figure 15c2). Once accommodation was healed, headward erosion formed a through-going incision across the slope profile (C4) (Figure 15c3,c4). Channel C4 was filled with sand up to the intermediate portion of the bypass-dominated zone, and then mud up-dip (Figure 11).

The different topographic profiles and the history of the FaSTaR cycles reflect the spatial and temporal evolution of the Marlim unit stepped slope. The slope profile during cycle 4 (a single step between two bypass-prone ramps, Figure 15c) suggests that the tilting, responsible for accommodation patterns and lateral stepping, was less active in step 1 at the end of the Marlim unit deposition, at least compared to the duration of the sediment supply cycle. The size of the lobate features, and their thickness and lithology suggest a substantial increase in the volume of sand bypassed and deposited from cycle 2 onwards.

5.4 | The FaSTaR model: A new stratigraphic model for dynamic stepped slope systems

The Marlim unit comprises several laterally associated FaSTaR cycles and multiple entry and exit points that progressively offset the NE. From this stratigraphic signature, we propose the FaSTaR model (Figure 16a), a new stratigraphic model that captures the high-resolution temporal and spatial evolution of connected slope depocentres in stepped slopes, in response to sediment supply fluctuations and lateral slope tilting. The sediment supply fluctuations are interpreted to respond to extra-basinal factors (i.e., sea-level changes/climate) that control the timing and duration of the waxing-to-waning sediment supply cycles and periods of sand starvation, whereas the lateral slope tilting is an intra-basinal factor that controls accommodation patterns during these cycles.

The FaSTaR model is different from the classic fill-and-spill model, which proposes a single fill-and-spill cycle or vertically stacked cycles to explain the stratigraphic

evolution of intra-slope basins with fixed topographic configurations and, therefore, with a fixed entry and exit point where sediment is bypassed towards the next downslope depocentre (e.g., Beaubouef & Friedmann, 2000; Pirmez et al., 2000; Prather, 2000; Prather et al., 1998; Sinclair & Tomasso, 2002; Smith, 2004; Winker, 1996) (Figure 16b). Another difference to the traditional fill-and-spill model are the incised channel complexes above step 1. The combination of a mild slope break from ramp 1 to step 1 and spatially limited accommodation in response to lateral tilting, prevented flows from forming more unconfined deposits such as distributary channels and lobes. These are more typical of static, undeforming, stepped slope systems or stepped slopes with vertical variation in accommodation patterns (e.g., Adeogba et al., 2005; Brooks et al., 2018; Deptuck et al., 2012; Hay, 2012; Spychala et al., 2015) (Figure 16).

Few studies document the impacts of lateral slope tilting on the evolution of deep-water deposition, and these focus on submarine channels affected by growing salt structures (e.g., Gee & Gawthorpe, 2006; Kane et al., 2012) and extensional faulting (e.g., Kane et al., 2010). However, lateral slope tilting may occur above any dynamic slope, which can be affected by a variety of structures, including fold-and-thrust belts, mud diapirs, salt tectonics and generic faulting. Therefore, given the prevalence of basins affected by mobile slopes around the world, we predict that the FaSTaR model is widely applicable to a range of settings where a component of lateral tilt is present. The relationship between tilting rate and sediment supply rate will ultimately dictate the emerging stratigraphic patterns. The model presented here shows an ordered record with complete fill-and-spill cycles intercalated with sand starvation periods. However, different rates and timing between controls could result in different signatures, for instance, incomplete cycles, lack of starvation periods or premature avulsions.

6 | CONCLUSIONS

This study uses 3D seismic reflection data calibrated to numerous wells and cores to document the stratigraphic evolution of the Marlim unit; a passive margin sand-prone stepped slope system active during the Oligocene–Miocene transition, which was deposited above a slow-moving tilting substrate affected by extensional salt tectonics. The model here proposed brings a new perspective on how stepped slope systems evolve. The main conclusions of this study are:

- Salt-related faulting and differential compaction (originated from underlying carbonate rafts) controlled the large-scale stepped slope configuration and, consequently, the location of depocentres and bypass-prone areas and sand distribution. The slope profile is formed by two steps connected by a TZ (ramp and corridor) and is bounded by two high-gradient ramps. Step 1 (up-dip) records low sinuosity incised channel complexes and remnant deposits of lobes, and step 2 (down-dip) records four lobate features formed by distributary channel and lobe complexes. The stratigraphic connection between the steps is supported by several bypass-dominated channels, later filled partially by mud and sand, which truncate deposits on the steps across the slope profile.
- Differences in architectural patterns, thickness and sandstone percentage in the steps suggest lateral variability in the magnitude of the slope breaks. The deposition of high sandstone percentage distributary channels and lobe complexes, locally thicker down-dip of the slope break, suggests abrupt slope breaks, whereas channelised deposits with moderate to high sandstone percentage support mild slope breaks.
- Seismic geomorphology and truncation patterns between the lobate features of step 2 support the unidirectional migration trend for the whole system. The shape, relative position and incisional relationships between the lobate features and the bypass-dominated channels that incise them support a unidirectional migration trend towards the NE in step 2. The stratigraphic link between the steps suggests the same trend for the laterally stepping channels interpreted in step 1.
- Several through-going bypass-dominated channels that enter and exit the steps in multiple locations indicate laterally associated fill-and-spill cycles (4 cycles in the case of the Marlim unit). These fill-and-spill cycles thicken to the NE. Moreover, these channels suggest that a local graded profile was achieved and that the sediment supply rate outpaced the deformation rate in each cycle. However, the mudstone fill of these incisions suggests a period of sediment supply reduction and sand starvation, reflecting fluctuations in the sediment supply cycles (waxing-waning) and channel abandonment.
- Lateral slope tilting is invoked as the mechanism to explain the thickness patterns, the accommodation creation for each cycle and the unidirectional migration trend of channel and lobe systems. As the lateral tilting component plays an essential role in the stratigraphic evolution, the cycles are here named FaSTaR (Fill-and-Spill, Tilt-and-Repeat) cycles.
- The repeated ordered pattern of accommodation filling and bypass in all the FaSTaR cycles is compatible with a constant rate of lateral tilting combined with sediment supply fluctuations. During periods of sand starvation

and long return periods between flows, the lateral tilt rate outpaced the sediment supply rate and the cumulative slope deformation induced channel avulsion at the start of a new FaSTaR cycle. Within each FaSTaR cycle, lateral connectivity and moderate to high sandstone percentage support short return periods between flows and relatively low rates of lateral tilting.

- 3D variability in the location and character of the slope breaks controlled the patterns of erosion and deposition and the evolution of each FaSTaR cycle. Three different slope configurations are proposed. FaSTaR cycles 1 and 2 evolved above two steps and three ramps, with step 1 being healed before step 2. During the FaSTaR cycle 3, deposition in the steps co-evolved since they were connected by a corridor and, during FaSTaR cycle 4, the slope profile comprised a single step edged by ramps.

This study demonstrates that fluctuations in sediment supply combined with comparatively low rates of syn-sedimentary lateral slope tilting produce distinctive depositional architecture that can help to inform the interplay of external and internal controls on a high-resolution scale. We provide a new model that predicts the stratigraphic signature of stepped slopes with vertical and lateral variation of accommodation patterns over time.

ACKNOWLEDGEMENTS

This study is part of the first author's PhD project, which is supported and funded by Petrobras S.A., Brazil. We thank Petrobras and the Brazilian National Agency of Petroleum, Natural Gas and Biofuels (ANP) for permission to use seismic and well data. Thais Cabral Almeida Empinotti, Tiago Agne de Oliveira and Iviana Setta Duarte are thanked for constructive feedback during the interpretation. We also thank the geoscientists of Petrobras' reservoir team for helping with the collation of data. We thank Pete Burgess as Editor and Bernard Dennielou and Brad Prather for perceptive reviews that have helped to improve the paper.

PEER REVIEW

The peer review history for this article is available at https://publons.com/publon/10.1111/bre.12700.

DATA AVAILABILITY STATEMENT

The data that support the findings of this study are property of the Brazilian National Agency of Petroleum, Natural Gas and Biofuels (ANP). Restrictions apply to the availability of these data, which were used under a research licence agreement between Petrobras and ANP. For more information about how to access geological and geophysical data from Brazilian Basins, contact helpdesk@anp.gov.br.

ORCID

Junia Casagrande https://orcid.org/0000-0002-3394-0301
David M. Hodgson https://orcid.org/0000-0003-3711-635X
Jeff Peakall https://orcid.org/0000-0003-3382-4578

REFERENCES

Adeogba, A. A., Mchargue, T. R., & Graham, S. A. (2005). Transient fan architecture and depositional controls from near-surface 3-D seismic data, Niger Delta continental slope. *AAPG Bulletin*, *89*, 627–643. https://doi.org/10.1306/11200404025

Albertão, G. A., Mulder, T., & Eschard, R. (2011). Impact of salt-related palaeotopography on the distribution of turbidite reservoirs: Evidence from well-seismic analyses and structural restorations in the Brazilian offshore. *Marine and Petroleum Geology*, *28*, 1023–1046. https://doi.org/10.1016/j.marpetgeo.2010.09.009

Alexander, J., & Morris, S. (1994). Observations on experimental, nonchannelized, high-concentration turbidity currents and variations in deposits around obstacles. *Journal of Sedimentary Research*, *64*, 899–909.

Allen, C., Gomis Cartesio, L. E., Hodgson, D. M., Peakall, J., & Milana, J.-P. (2022). Channel incision into a submarine landslide on a carboniferous basin margin, San Juan, Argentina: Evidence for the role of knickpoints. *The Depositional Record*, *8*, 628–655. https://doi.org/10.1002/dep2.178

Barton, M. D. (2012). Evolution of an intra-slope apron, offshore Niger Delta slope: Impact of step geometry on apron architecture. In B. E. Prather, M. E. Deptuck, D. C. Mohrig, B. van Hoorn, & R. B. Wynn (Eds.), *Application of the principles of seismic geomorphology to continental-slope and base-of-slope systems: Case studies from seafloor and near-seafloor analogue* (Vol. *99*, pp. 181–197). SEPM Special Publication.

Beaubouef, R. T., & Friedmann, S. J. (2000). High resolution seismic/sequence stratigraphic framework for the evolution of Pleistocene intra slope basins, western Gulf of Mexico: Depositional models and reservoir analogs. In P. Weimer, R. M. Slatt, J. Coleman, N. C. Rosen, H. Nelson, A. H. Bouma, M. J. Styzen, & D. T. Lawrence (Eds.), *Deep-water reservoirs of the world: 20th annual gulf coast section* (pp. 40–60). SEPM Foundation, Bob F. Perkins Research Conference.

Beddow, H. M., Liebrand, D., Sluijs, A., Wade, B. S., & Lourens, L. J. (2016). Global change across the Oligocene-Miocene transition: High-resolution stable isotope records from IODP site U1334 (equatorial Pacific Ocean). *Paleoceanography*, *31*, 81–97. https://doi.org/10.1002/2015PA002820

Booth, J. R., Dean, M. C., DuVernay, A. E., III, & Styzen, M. J. (2003). Paleo-bathymetric controls on the stratigraphic architecture and reservoir development of confined fans in the Auger Basin: Central Gulf of Mexico slope. *Marine and Petroleum Geology*, *20*, 563–586. https://doi.org/10.1016/j.marpetgeo.2003.03.008

Brooks, H. L., Hodgson, D. M., Brunt, R. L., Peakall, J., Poyatos-Moré, M., & Flint, S. S. (2018). Disconnected submarine lobes as a record of stepped slope evolution over multiple sea-level cycles. *Geosphere*, *14*, 1753–1779. https://doi.org/10.1130/GES01618.1

Bruhn, C. H. L. (1998). *Deep-water reservoirs from the eastern Brazilian rift and passive margin basins*. AAPG International Conference and Exhibition, Rio de Janeiro, Brazil, AAPG Short Couse Notes, Part 2, p. 191.

Bruhn, C. H. L., Gomes, J. A. T., Del Lucchese, C., Jr., & Johann, P. R. S. (2003). Campos Basin: Reservoir characterization and management - historical overview and future challenges. In *Offshore Technology Conference 15220-MS*, Houston, Texas. https://doi.org/10.4043/15220-ms

Bruhn, C. H. L., Pinto, A. C. C., Johann, P. R. S., Branco, C. C. M., Salomão, M. C., & Freire, E. B. (2017). Campos and Santos basins: 40 years of reservoir characterization and management of shallow- to ultra-deep water, post- and pre-salt reservoirs—Historical overview and future challenges. In *Offshore Technology Conference 28159-MS*, Rio de Janeiro, Brazil. https://doi.org/10.4043/28159-MS

Cainelli, C., & Mohriak, W. U. (1999). Some remarks on the evolution of sedimentary basins along the eastern Brazilian continental margin. *Episodes*, *22*, 206–216.

Castro, R. D., & Picolini, J. P. (2015). Main features of the Campos Basin regional geology. In R. O. Kowsmann (Ed.), *Geology and geomorphology* (Vol. *1*, pp. 1–12). Habitats.

Chang, H. K., Kowsmann, R. O., Figueiredo, A. M. F., & Bender, A. (1992). Tectonics and stratigraphy of the East Brazil rift system: An overview. *Tectonophysics*, *213*, 97–138.

Chima, K. I., Do Couto, D., Leroux, E., Gardin, S., Hoggmascall, N., Rabineau, M., Granjeon, D., & Gorini, C. (2019). Seismic stratigraphy and depositional architecture of neogene intraslope basins, offshore western Niger Delta. *Marine and Petroleum Geology*, *109*, 449–468. https://doi.org/10.1016/j.marpetgeo.2019.06.030

Christie, D. N., Peel, F. J., Apps, G. M., & Stanbrook, D. S. (2021). Forward modelling for structural stratigraphic analysis, offshore Sureste Basin, Mexico. *Frontiers in Earth Science*, *9*, 767329. https://doi.org/10.3389/feart.2021.767329

Cobbold, P. R., & Szatmari, P. (1991). Radial gravitational gliding on passive margins. *Tectonophysics*, *188*, 249–289. https://doi.org/10.1016/0040-1951(91)90459-6

Collier, R. E. L. (1991). The lower carboniferous Stainmore Basin, N. England: Extensional basin tectonics and sedimentation. *Journal of the Geological Society of London*, *148*, 379–390.

Cumberpatch, Z. A., Kane, I. A., Soutter, E. L., Hodgson, D. M., Jackson, C. A.-L., Kilhams, B. A., & Poprawski, Y. (2021). Interactions of deep-water gravity flows and active salt tectonics. *Journal of Sedimentary Research*, *91*, 34–65. https://doi.org/10.2110/jsr.2020.047

De Gasperi, A., & Catuneanu, O. (2014). Sequence stratigraphy of the Eocene turbidite reservoirs in Albacora field, Campos Basin, offshore Brazil. *AAPG Bulletin*, *98*(2), 279–313.

Demercian, S., Szatmari, P., & Cobbold, P. R. (1993). Style and pattern of salt diapirs due to thin-skinned gravitational gliding, Campos and Santos basins, offshore Brazil. *Tectonophysics*, *228*(3–4), 393–433. https://doi.org/10.1016/0040-1951(93)90351-J

Deptuck, M. E., Sylvester, Z., & O'Byrne, C. (2012). Pleistocene seascape evolution above a "simple" stepped slope–Western Niger Delta. In B. E. Prather, M. E. Deptuck, D. C. Mohrig, B. van Hoorn, & R. B. Wynn (Eds.), *Application of the principles of seismic geomorphology to continental-slope and base-of-slope systems: Case studies from seafloor and near-seafloor analogue* (Vol. *99*, pp. 199–222). SEPM Special Publication. https://doi.org/10.2110/pec.12.99

Doughty-Jones, G., Mayall, M., & Lonergan, L. (2017). Stratigraphy, facies, and evolution of deep-water lobe complexes within a salt-controlled intraslope minibasin. *AAPG Bulletin*, *101*, 1879–1904. https://doi.org/10.1306/01111716046

do Amarante, F. B., Jackson, C. A.-L., Pichel, L. M., Scherer, C. M. S., & Kuchle, J. (2021). Pre-salt rift morphology controls salt tectonics in the Campos Basin, offshore SE Brazil. *Basin Research*, *33*, 2837–2861. https://doi.org/10.1111/bre.12588

Duval, B., Cramez, C., & Jackson, M. P. A. (1992). Raft tectonics in the Kwanza Basin, Angola. *Marine and Petroleum Geology*, *9*, 389–404. https://doi.org/10.1016/0264-8172(92)90050-O

Fetter, M. (2009). The role of basement tectonic reactivation on the structural evolution of Campos Basin, offshore Brazil: Evidence from 3D seismic analysis and section restoration. *Marine and Petroleum Geology*, *26*, 873–886. https://doi.org/10.1016/j.marpetgeo.2008.06.005

Fetter, M., De Ros, L. F., & Bruhn, C. H. L. (2009). Petrographic and seismic evidence for the depositional setting of giant turbidite reservoirs and the palaeogeographic evolution of Campos Basin, offshore Brazil. *Marine and Petroleum Geology*, *26*(6), 824–853.

Garcia, M., & Parker, G. (1989). Experiments on hydraulic jumps in turbidity currents near a canyon-fan transition. *Science*, *245*, 393–396.

Gee, M. J. R., & Gawthorpe, R. L. (2006). Submarine channels controlled by salt tectonics: Examples from 3D seismic data offshore Angola. *Marine and Petroleum Geology*, *23*, 443–458.

Guardado, L. R., Spadini, A. R., Brandão, J. S. L., & Mello, M. R. (2000). Petroleum system of the Campos Basin. In M. R. Mello & B. J. Katz (Eds.), *Petroleum systems of South Atlantic margins* (Vol. *73*, pp. 317–324). AAPG Memoir.

Guiastrennec-Faugas, L., Gillet, H., Peakall, J., Silva Jacinto, R., & Dennielou, B. (2021). Initiation and evolution of knickpoints and their role in cut and fill processes in active submarine channels. *Geology*, *49*, 314–319. https://doi.org/10.1130/G48369.1

Haughton, P., Davis, C., McCaffrey, W., & Barker, S. (2009). Hybrid sediment gravity flow deposits—Classification, origin and significance. *Marine and Petroleum Geology*, *26*, 1900–1918.

Hay, D. C. (2012). Stratigraphic evolution of a tortuous corridor from the stepped slope of Angola. In E. Bradford, M. D. Prather, D. Mohrig, B. van Hoorn, & R. B. Wynn (Eds.), *Application of the principles of seismic geomorphology to continental-slope and base-of-slope systems: Case studies from seafloor and near-seafloor analogues* (Vol. *99*, pp. 163–180). SEPM Special Publication.

Heijnen, M. S., Clare, M. A., Cartigny, M. J. B., Talling, P. J., Hage, S., Lintern, D. G., Stacey, C., Parsons, D. R., Simmons, S. M., Chen, Y., Sumner, E. J., Dix, J. K., & Hughes Clarke, J. E. (2020). Rapidly-migrating and internally-generated knickpoints can control submarine channel evolution. *Nature Communications*, *11*, 3129.

Hodgson, D. M. (2009). Distribution and origin of hybrid beds in sand-rich submarine fans of the Tanqua depocentre, Karoo Basin, South Africa. *Marine and Petroleum Geology*, *26*, 1940–1956.

Hodgson, D. M., Di Celma, C. N., Brunt, R. L., & Flint, S. S. (2011). Submarine slope degradation and aggradation and the stratigraphic evolution of channel-levee systems. *Journal of the Geological Society of London*, *168*, 625–628. https://doi.org/10.1144/0016-76492010-177

Howlett, D. M., Gawthorpe, R. L., Ge, Z., Rotevatn, A., & Jackson, C. A.-L. (2021). Turbidites, topography and tectonics: Evolution of

submarine channel-lobe systems in the salt-influenced Kwanza Basin, offshore Angola. *Basin Research*, *33*, 1076–1110. https://doi.org/10.1111/bre.12506

Jackson, C. A.-L., Barber, G. P., & Martinsen, O. J. (2008). Submarine slope morphology as a control on the development of sand-rich turbidite depositional systems: 3D seismic analysis of the Kyrre Fm (upper cretaceous), Maloy slope, offshore Norway. *Marine and Petroleum Geology*, *25*, 663–680. https://doi.org/10.1016/j.marpetgeo.2007.12.007

Jackson, C. A. L., McAndrew, A. E., Hodgson, D. M., & Dreyer, T. (2021). Repeated degradation and progradation of a submarine slope over geological time scales. *Journal of Sedimentary Research*, *91*, 116–145. https://doi.org/10.2110/jsr.2020.77

Jackson, M. P. A., & Hudec, M. R. (2017). *Salt tectonics: Principles and practice*. Cambridge University Press. https://doi.org/10.1017/9781139003988

Jobe, Z. R., Sylvester, Z., Howes, N., Pirmez, C., Parker, A., Cantelli, A., Smith, R., Wolinsky, M. A., O'Byrne, C., Slowey, N., & Prather, B. (2017). High-resolution, millennial-scale patterns of bed compensation on a sand-rich intraslope submarine fan, western Niger Delta slope. *Geological Society of America Bulletin*, *129*, 23–37.

Kane, I. A., Catterall, V., McCaffrey, W. D., & Martinsen, O. J. (2010). Submarine channel response to intra-basinal tectonics. *AAPG Bulletin*, *94*, 189–219.

Kane, I. A., McGee, D. T., & Jobe, Z. R. (2012). Halokinetic effects on submarine channel equilibrium profiles and implications for facies architecture: Conceptual model illustrated with a case study from Magnolia field, Gulf of Mexico. In G. I. Alsop, S. G. Archer, A. J. Hartley, N. T. Grant, & R. Hodgkinson (Eds.), *Salt tectonics, sediments and prospectivity* (Vol. *363*, pp. 289–302). Geological Society of London Special Publication.

Kane, I. A., Ponten, A. S. M., Vangdal, B., Eggenhuisen, J. T., Hodgson, D. M., & Spychala, Y. T. (2017). The stratigraphic record and processes of turbidity current transformation across deep-marine lobes. *Sedimentology*, *64*, 1236–1273.

Kneller, B. C., & McCaffrey, W. D. (1999). Depositional effects of flow non- uniformity and stratification within turbidity currents approaching a bounding slope: Deflection, reflection and facies variation. *Journal of Sedimentary Research*, *69*, 980–991. https://doi.org/10.2110/jsr.69.980

Kubo, Y. S. (2004). Experimental and numerical study of topographic effects on deposition from two-dimensional, particle-driven density currents. *Sedimentary Geology*, *164*, 311–326.

Li, P., Kneller, B., & Hansen, L. (2021). Anatomy of a gas-bearing submarine channel-lobe system on a topographically complex slope (offshore Nile Delta, Egypt). *Marine Geology*, *437*, 106496.

Mayall, M., Lonergan, L., Bowman, A., James, S., Mills, K., Primmer, T., Pope, D., Rogers, L., & Skeene, R. (2010). The response of turbidite slope channels to growth-induced seabed topography. *AAPG Bulletin*, *94*, 1011–1030. https://doi.org/10.1306/01051009117

Meckel, L. D., III, Ugueto, G. A., Lynch, H. D., Cummings, E. W., Hewett, B. M., Bogage, E. J., Winker, C. D., & O'Neil, B. J. (2002). Genetic stratigraphy, stratigraphic architecture, and reservoir stacking patterns of the upper Miocene-lower Pliocene greater Mars-Ursa intraslope basin, Mississippi canyon, Gulf of Mexico. In J. M. Armentrout & N. C. Rosen (Eds.), *Sequence stratigraphic models for exploration and production: Evolving methodology, emerging models, and application histories: 22nd annual gulf coast section* (pp. 113–147). SEPM Foundation, Bob F. Perkins Research Conference.

Mignard, S., Mulder, T., Martinez, P., & Garlan, T. (2019). The Ogooue fan (offshore Gabon): A modern example of deep-sea fan on a complex slope profile. *Solid Earth*, *10*(3), 851–869.

Mohriak, W. U., Basseto, M., & Vieira, I. S. (1998). Crustal architecture and tectonic evolution of the Sergipe-Alagoas and Jacuipe basins, offshore northeastern Brazil. *Tectonophysics*, *288*, 199–220.

Mohriak, W., Nemčok, M., & Enciso, G. (2008). South Atlantic divergent margin evolution: Rift-border uplift and salt tectonics in the basins of SE Brazil. *Geological Society, London, Special Publications*, *294*, 365–398. https://doi.org/10.1144/sp294.19

Mohriak, W. U., Szatmari, P., & Anjos, S. (2012). Salt: Geology and tectonics of selected Brazilian basins in their global context. *Geological Society, London, Special Publications*, *363*, 131–158. https://doi.org/10.1144/sp363.7

Moraes, M. A. S., Maciel, W. B., Braga, M. S. S., & Viana, A. R. (2007). Bottom-current reworked Palaeocene-Eocene deep-water reservoirs of the Campos Basin, Brazil. In A. R. Viana & M. Rebesco (Eds.), *Economic and palaeoceanographic significance of contourite deposits* (Vol. *276*, pp. 81–94). Geological Society, Special Publications.

Morris, S. A., & Alexander, J. (2003). Changes in flow direction at a point caused by obstacles during passage of a density current. *Journal of Sedimentary Research*, *73*, 621–629.

Mulder, T., & Alexander, J. (2001). Abrupt change in slope causes variation in the deposit thickness of concentrated particle-driven density currents. *Marine Geology*, *175*, 221–235.

Oluboyo, A. P., Gawthorpe, R. L., Bakke, K., & Hadler-Jacobsen, F. (2014). Salt tectonic controls on deep-water turbidite depositional systems: Miocene, southwestern lower Congo basin, offshore Angola. *Basin Research*, *26*, 597–620. https://doi.org/10.1111/bre.12051

Peakall, J., McCaffrey, B., Kneller, B., Stelting, C. E., McHargue, T. R., & Schweller, W. J. (2000). A process model for the evolution of submarine fan channels: Implications for sedimentary architecture. In A. H. Bouma & C. G. Stone (Eds.), *Fine-grained turbidite systems* (Vol. *72*, pp. 73–89). AAPG Memoir.

Peakall, J., McCaffrey, W. D., & Kneller, B. C. (2000). A process model for the evolution, morphology and architecture of sinuous submarine channels. *Journal of Sedimentary Research*, *70*, 434–448.

Peakall, J., Leeder, M. R., Best, J. L., & Ashworth, P. J. (2000). River response to lateral ground tilting: A synthesis and some implications for the modelling of alluvial architecture in extensional basins. *Basin Research*, *12*, 413–424.

Pirmez, C., Beaubouef, R. T., Friedmann, S. J., & Mohrig, D. C. (2000). Equilibrium profile and base level in submarine channels: Examples from Late Pleistocene systems and implications for the architecture of deep-water reservoirs. In P. Weimer, R. M. Slatt, J. Coleman, N. C. Rosen, H. Nelson, A. H. Bouma, M. J. Styzen, & D. T. Lawrence (Eds.), *Deep-water reservoirs of the world: 20th annual gulf coast section* (pp. 782–805). SEPM Foundation, Bob F. Perkins Research Conference.

Prather, B. E., Booth, J. R., Steffens, G. S., & Craig, P. A. (1998). Classification, lithologic calibration and stratigraphic succession of seismic facies from intraslope basins, deep water Gulf of Mexico, USA. *AAPG Bulletin*, *82*, 701–728.

Prather, B. E. (2000). Calibration and visualization of depositional process models for above-grade slopes: A case study from the Gulf of Mexico. *Marine and Petroleum Geology*, *17*(5), 619–638.

Prather, B. E. (2003). Controls on reservoir distribution, architecture and stratigraphic trapping in slope settings. *Marine and Petroleum Geology*, *20*, 529–545. https://doi.org/10.1016/j.marpetgeo.2003.03.009

Prather, B. E., O'Byrne, C. J., Pirmez, C., & Sylvester, Z. (2009). Sediment partitioning across Tertiary continental slopes AAPG search and discovery article #90090. AAPG annual convention and exhibition, Denver, Colorado, June 7-10 2009. In: Abstracts, CD American Association of Petroleum Geologists.

Prather, B. E., Pirmez, C., Sylvester, Z., & Prather, D. S. (2012). Stratigraphic response to evolving geomorphology in a submarine apron perched on the upper Niger delta slope. In B. E. Prather, M. E. Deptuck, D. C. Mohrig, B. van Hoorn, & R. B. Wynn (Eds.), *Application of the principles of seismic geomorphology to continental-slope and base-of-slope systems: Case studies from seafloor and near-seafloor analogue* (Vol. *99*, pp. 145–161). SEPM Special Publication.

Prather, B. E., Pirmez, C., & Winker, C. D. (2012). Stratigraphy of linked Intraslope basins: Brazos–trinity system Western Gulf of Mexico. In B. E. Prather, M. E. Deptuck, D. C. Mohrig, B. van Hoorn, & R. B. Wynn (Eds.), *Application of the principles of seismic geomorphology to continental-slope and base-of-slope systems: Case studies from seafloor and near-seafloor analogue* (Vol. *99*, pp. 83–109). SEPM Special Publication.

Privat, A. M.-L., Hodgson, D. M., Jackson, C. A.-L., Schwarz, E., & Peakall, J. (2021). Evolution from syn-rift carbonates to early post-rift deep-marine intraslope lobes: The role of rift basin physiography on sedimentation patterns. *Sedimentology*, *68*, 2563–2605. https://doi.org/10.1111/sed.12864

Quirk, D. G., Schødt, N., Lassen, B., Ings, S. J., Hsu, D., Hirsch, K. K., & Von Nicolai, C. (2012). Salt tectonics on passive margins: Examples from Santos, Campos and kwanza basins. *Geological Society, London, Special Publications*, *363*, 207–244. https://doi.org/10.1144/sp363.10

Rangel, H. D., & Martins, C. C. (1998). Principais compartimentos exploratórios, Bacia de Campos. In M. Taha (Ed.), *Cenário Geológico nas Bacias Sedimentares no brasil. The search-searching for oil and gas in the land of giants* (Vol. *2*, pp. 32–40). Special Publication.

Sinclair, H. D., & Tomasso, M. (2002). Depositional evolution of confined turbidite basins. *Journal of Sedimentary Research*, *72*, 451–456. https://doi.org/10.1306/111501720451

Smith, R. (2004). Silled sub-basins to connected tortuous corridors: Sediment distribution system on topographically complex subaqueous slopes. In S.A. Lomas and P. Joseph, (Eds.), *Confined turbidite systems* (Vol. *222*, pp. 23–43). Geological Society of London, Special Publication.

Southern, S. J., Kane, I. A., Warchoł, M. J., Porten, K. W., & McCaffrey, W. D. (2017). Hybrid event beds dominated by transitional-flow facies: Character, distribution and significance in the Maastrichtian Springar formation, north-west Vøring Basin, Norwegian Sea. *Sedimentology*, *64*, 747–776.

Spychala, Y. T., Hodgson, D. M., Flint, S. S., & Mountney, N. P. (2015). Constraining the sedimentology and stratigraphy of submarine intraslope lobe deposits using exhumed examples from the Karoo Basin, South Africa. *Sedimentary Geology*, *322*, 67–81. https://doi.org/10.1016/j.sedgeo.2015.03.013

Spychala, Y. T., Eggenhuisen, J. T., Tilston, M., & Pohl, F. (2020). The influence of basin setting and turbidity current properties on the dimensions of submarine lobe elements. *Sedimentology*, *67*, 3471–3491.

Stevenson, C. J., Talling, P. J., Wynn, R. B., Masson, D. G., Hunt, J. E., Frenz, M., Akhmetzhanhov, A., & Cronin, B. T. (2013). The flows that left no trace: Very large volume turbidity currents that bypassed sediment through submarine channels without eroding the sea floor. *Marine and Petroleum Geology*, *41*, 186–205.

Stevenson, C. J., Jackson, C. A.-L., Hodgson, D. M., Hubbard, S. M., & Eggenhuisen, J. (2015). Deep-water sediment bypass. *Journal of Sedimentary Research*, *85*, 1058–1081.

Steventon, M. J., Jackson, C. A. L., Johnson, H. D., Hodgson, D. M., Kelly, S., Omma, J., Gopon, C., Stevenson, C., & Fitch, P. (2021). Evolution of a sand-rich submarine channel–lobe system, and the impact of mass-transport and transitional-flow deposits on reservoir heterogeneity: Magnus field, northern North Sea. *Petroleum Geoscience*, *27*, 2020–2095. https://doi.org/10.1016/j.marpetgeo.2006.01.002

Straub, K. M., Paola, C., Mohrig, D., Wolinsky, M. A., & George, T. (2009). Compensational stacking of channelized sedimentary deposits. *Journal of Sedimentary Research*, *79*(9), 673–688.

Sylvester, Z., Cantelli, A., & Pirmez, C. (2015). Stratigraphic evolution of intraslope minibasins: Insights from surface-based model. *AAPG Bulletin*, *99*, 1099–1129.

Tek, D. E., McArthur, A. D., Poyatos-Moré, M., Colombera, L., Patacci, M., Craven, B., & McCaffrey, W. D. (2021). Relating seafloor geomorphology to subsurface architecture: How mass-transport deposits and knickpoint-zones build the stratigraphy of the deep-water Hikurangi Channel. *Sedimentology*, *68*, 3141–3190.

Wang, X., Luthi, S. M., Hodgson, D. M., Sokoutis, D., Willingshofer, E., & Groenenberg, R. M. (2017). Turbidite stacking patterns in salt-controlled minibasins: Insights from integrated analogue models and numerical fluid flow simulations. *Sedimentology*, *64*, 530–552.

Winker, C. D. (1996). High resolution seismic stratigraphy of a late Pleistocene submarine fan ponded by salt-withdrawal minibasins on the Gulf of Mexico continental slope. In *Offshore Technology Conference 8024* (pp. 619–628).

Winter, W. R., Jahnert, R. J., & França, A. B. (2007). Bacia de Campos. *Boletim de Geociências da Petrobras*, *15*(2), 511–529.

Wu, N., Jackson, C. A. L., Johnson, H. D., Hodgson, D. M., & Nugraha, H. D. (2020). Mass-transport complexes (MTCs) document subsidence patterns in a northern Gulf of Mexico salt minibasin. *Basin Research*, *32*, 1300–1327. https://doi.org/10.1111/bre.12429

How to cite this article: Casagrande, J., Hodgson, D. M., Peakall, J., & Benac, P. M. (2022). Fill-and-Spill, Tilt-and-Repeat (FaSTaR) cycles: Stratigraphic evolution above a dynamic submarine stepped slope. *Basin Research*, *34*, 2162–2188. https://doi.org/10.1111/bre.12700